Journal of Structural Geology 94 (2017) 13–31

Contents lists available at ScienceDirect

Journal of Structural Geology

journal homepage: www.elsevier.com/locate/jsg

Newly identified active faults in the Pollino seismic gap, southern Italy, and their seismotectonic significance

Francesco Brozzetti [a, *], Daniele Cirillo [a], Rita de Nardis [a, b], Mauro Cardinali [c], Giusy Lavecchia [a], Barbara Orecchio [d], Debora Presti [d], Cristina Totaro [d]

[a] CRUST, DiSPUTer - Università G. d'Annunzio, Via dei Vestini, 66100, Chieti, Italy
[b] Dipartimento della Protezione Civile, Via Vitorchiano 4, 00189, Rome, Italy
[c] CNR IRPI Perugia, Via della Madonna Alta, 126, 06128, Perugia, Italy
[d] Dipartimento di Scienze Matematiche e Informatiche, Scienze Fisiche e Scienze della Terra - Università di Messina, Viale F. Stagno D'Alcontres, 98166, Messina, Italy

ARTICLE INFO

Article history:
Received 23 February 2016
Received in revised form
4 October 2016
Accepted 23 October 2016
Available online 24 October 2016

Keywords:
Quaternary and active extensional faults
Earthquakes location
Earthquake/fault association
Seismogenic style
Southern Italy

ABSTRACT

The following is a geological study of a Quaternary and active normal fault-system, which crops out in the Pollino area, a seismogenic sector of the Southern Apennines, Italy.

From 2010 to 2014, this area was affected by long lasting seismic activity characterized by three major events which occurred in May 2012 (Mw 4.3), in October 2012 (Mw 5.2) and in June 2014 (Mw 4.0). The integration of structural-geological data with morpho-structural and remote sensing analyses, led to define the geometry, the kinematics, the cross-cutting relationships and the slip rates of the inferred active fault segments within and near the epicentral area.

We reconstructed an asymmetric extensional pattern characterized by low-angle, E and NNE-dipping faults, and by antithetic, high-angle, SW- to WSW-dipping faults. The geometry of the faults at depth was constrained using high-resolution hypocenter distributions. The overall system fits well with the deformation field obtained from focal mechanisms and geodetic data.

Comparing the fault pattern with the time-space evolution of the Pollino seismic activity, we identified the seismogenic sources in two, near-parallel, WSW-dipping faults, whose seismogenic potential were assessed.

The peculiar perpendicular-to-fault-strike evolution of the seismic activity, is discussed in the frame of the reconstructed seismotectonic model.

1. Introduction

In structurally complex regions characterized by polyphasic tectonic history, the identification of active and potentially seismogenic structures, using only surface geology criteria, becomes an arduous task. A high level of uncertainty mainly characterizes the regions affected by low strain rates, in which the effects of active faulting on topography are not clear, the coseismic surface ruptures are rare or lacking, and their interpretation is controversial.

On the other hand, only the seismology and/or geophysics may not be decisive in this matter. The reasons could be due to:

i) most of regional-scale normal and thrust faults display an irregular 3D shape (Bally and Snelson, 1980; Wernicke and Burchfiel, 1982; Suppe, 1983; Gibbs, 1984 among many others) that cannot be determined in absence of large dataset of subsurface data (e.g. 3D grid of seismic reflection profiles and well data) and makes the correlation uncertain between the hypocentral locations and the outcropping fault;
ii) very shallow-depth earthquakes (2 km or less) are rare and/or very badly located, hampering the "direct" link between the fault trace and the clusters of hypocenter locations;
iii) the geological and seismological datasets may have different degrees of accuracy, making their reciprocal correlation difficult (Jackson and White, 1989; Collettini and Sibson, 2001).

* Corresponding author.
E-mail address: f.brozzetti@dst.unich.it (F. Brozzetti).

http://dx.doi.org/10.1016/j.jsg.2016.10.005

This study highlights the fact that where a significant seismic crisis occurs, even if it lacks some significant and probative data, as surface ruptures, paleoseismological trenches or offset of very recent sediments, the full integration of high-quality structural-geological and seismological data can help to overcome the above uncertainties, leading to the identification and parameterization of the activated individual sources.

A two-step methodology is proposed, considered useful also in poorly understood regions, based on the comparison between 1) a detailed structural-geological survey, integrated with morpho-structural analyses as the basic instruments for identifying the faults that have a "fresh" geomorphic signature and are geometrically and kinematically compatible with the distribution of seismicity and 2) datasets of high-quality relocated earthquakes, possibly recorded through a dedicated temporary network, which is representative of the entire evolution of the seismic sequence.

An interesting case concerns the Mt. Pollino region, located in Southern Italy, on the Calabria-Lucania border between the Apennines s.s. and the Calabrian arc (Fig. 1a). The Pollino region is part of a silent sector of the intra-Apennine seismogenic belt, considered a persistent seismic gap (Cinti et al., 1997; Michetti et al., 1997; Chiarabba et al., 2016), struck by a four-year lasting (2010–2014) moderate seismic sequence (maximum magnitude up to M_w 5.2, Totaro et al., 2015).

The seismotectonic setting of the region is particularly complex because of the superposition, from the uppermost Early Pleistocene, of a low strain-rate extensional deformation (Hunstad et al., 2003; D'Agostino et al., 2013) over pre-exiting strike-slip Late Pliocene-Early Pleistocene structures (Bousquet and Gueremy, 1969; Ghisetti and Vezzani, 1982; Schiattarella, 1998; Schiattarella et al., 1994; Knott and Turco, 1991).

A large number of normal faults, some of which associated to a displacement exceeding 1000 m, generated during both the strike-slip and the extensional tectonic phases, giving rise to articulated fault systems. Furthermore, during the Quaternary, the region underwent an uplift with rates of ~1.2–1.3 mm/yr (Schiattarella et al., 2003, 2006; Gioia et al., 2011), due to extensional tectonics coupled with thermal/isostatic raising, which caused the exhumation of a number of fault planes, some of which cropping out with apparently fresh free faces.

On one hand, the geological complexities, and on the other, the low and sparse instrumental seismicity, made the distinction between the presently active and inactive structures very complicated and led to conflicting interpretations (Schiattarella et al., 1994; Michetti et al., 1997; Papanikolaou and Roberts, 2007; Brozzetti et al., 2009; Spina et al., 2009).

When the Pollino region was affected by the 2010–2014 seismic crisis, the discrepancy between the pattern of the faults referred as active in previous studies (Michetti et al., 2000; Papanikolaou and Roberts, 2007; Faure Walker et al., 2012), and the distribution of the seismicity was evident (Passarelli et al., 2015).

In this paper, a previously unidentified and only partially mapped, Late Quaternary extensional fault system will be reconstructed and a corresponding digital database elaborated. The integration of the newly acquired geological data, with high-resolution seismological locations (Totaro et al., 2015) will make the deep reconstruction of the individual fault segments possible. The defined seismotectonic model will be also useful to give new insights on the kinematics and the structural style of the active deformation in this enigmatic area, improving our understanding of seismic hazard scenarios.

In fact, although the 2010–2014 Pollino seismic sequence only released moderate events, the recognition of the related seismogenic fault pattern is particularly relevant in light of the high seismogenic potential of the region, capable of generating earthquakes up to a magnitude of 7 (Rovida et al., 2011; Michetti et al., 1997, 2000; Cinti et al., 1997, 2002).

The results of this work stress that in areas affected by a complex fault array, and struck by moderate-magnitude earthquakes, as in the Pollino case, only a fully integrated geological-seismological approach could be decisive in order to constrain the active and seismogenic deformation pattern.

1.1. Regional seismotectonic setting

This study focuses on the active tectonics of the western side of Mt. Pollino massif, in the western part of the Calabro-Lucanian Apennines (Fig. 1 and 2) which originated during the Neogene due to the consumption of the Tethyan domain and the subsequent compression of the western Adria Plate (D'Argenio, 1992; Patacca and Scandone, 2007 and attached references). In the study area, the two shallowest, tectonic units of the Southern Apennines edifice crop out. From the uppermost, they are referred to as the Ligurian Unit and the Apennines Platform (Figs. 2 and 3). The Ligurian Unit derives from the Ligurian Basin, originally located on the west of the Adria continental margin. It consists mainly of metapelites and metarenites of the Early Cretaceous age (Ghisetti and Vezzani, 1983; Ietto and Ietto, 2011). The Apennine Platform is a >4 km-thick carbonate shelf succession, ranging from Upper Triassic to Middle Miocene (Amodio Morelli et al., 1976; Ogniben, 1969), that can be separated in a western margin-to-slope facies, represented by the Verbicaro Unit and in a persistent lagoon facies, represented by the Pollino Unit. In the study area, the Verbicaro Unit, that exhibits a HP-LT metamorphism whose imprint increases towards the South (Iannace et al., 2005, 2007; Rossetti et al., 2004; Patacca and Scandone, 2007) is stacked over the Pollino Unit with a minimum horizontal displacement of 20 km (Ghisetti and Vezzani, 1983) (Fig. 3a and b). Its major outcrops occur in the Calabria Coastal Range and along the South-Western margin of the Pollino ridge also referred to as San Donato Metamorphic core (Pierattini et al., 1975; Dietrich et al., 1976; Ietto and Barilaro, 1993).

The compressional structures of the Verbicaro and the Pollino Units, of Early to Middle Miocene age, were first displaced by a set of WNW-ESE-striking regional strike-slip faults characterized by left-lateral kinematics during the Middle Miocene-Late Pliocene time span (Grandjacquet, 1962; Ghisetti and Vezzani, 1982; Van Dijk et al., 2000) and by alignments of East- and West-dipping normal faults (light blue domain in Fig. 1b; Brozzetti, 2011), some of which are considered active and seismogenic (Michetti et al., 1997; Cinti et al., 1997, 2002; Papanikolaou and Roberts, 2007; Brozzetti et al., 2009). Along the Tyrrhenian side, the extensional belt is bound by regional, East-dipping normal faults which have been recognized from Campania to the north of Calabria (Fig. 1a and b; Brozzetti, 2011).

Several Quaternary intra-mountain continental basins developed all along the extensional domain. Their formation was mainly influenced by both the West-dipping faults (Vallo di Diano and Mercure Basins) and the East-dipping ones (Auletta and Melandro-Pergola basins) (Fig. 1a). The East-and West-dipping Quaternary fault arrays control the distribution of major seismicity on a regional scale, as shown by upper crustal instrumental earthquakes (ISIDe database, Working Group INGV, 2015 and by the distribution of destructive historical events (Fig. 1a, Rovida et al., 2011). The overall seismogenic fault system is kinematically compatible with a SW-NE direction of extension provided by the focal mechanisms of the major events (earthquakes in Fig. 1b and reference therein). An ongoing, nearly SW-NE extension, affecting the belt is also highlighted by recent GPS data from permanent and temporary stations (D'Agostino et al., 2013, Fig. 1b).

In the study area, SW-dipping normal faults (Figs. 1c and 2),

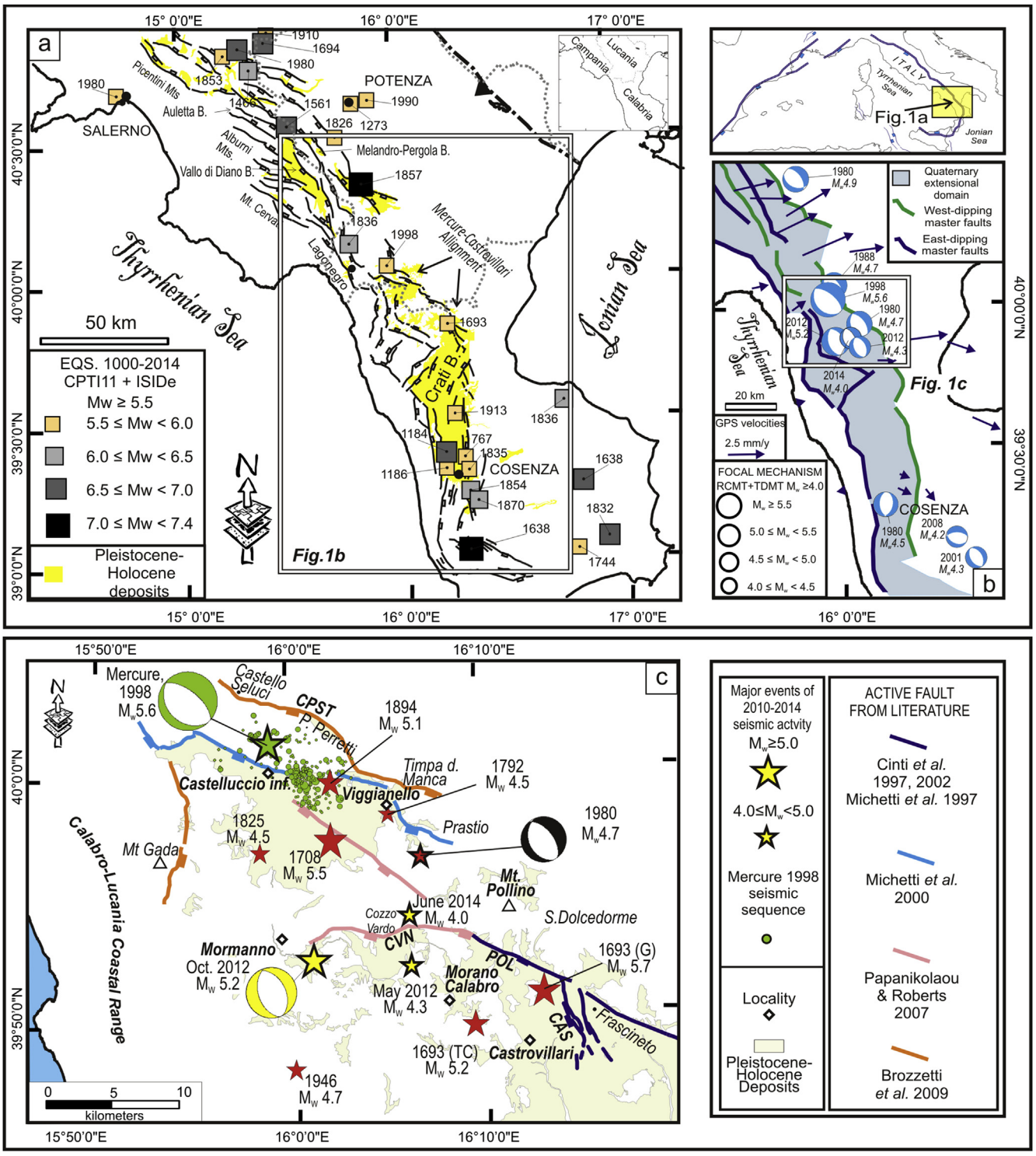

Fig. 1. Regional seismotectonic framework of the Pollino 2010–2014 seismic activity. (a) Structural map of the Quaternary normal faults and associated syn-sedimentary basins (yellow areas) in southern Italy (after Brozzetti et al., 2009; Brozzetti, 2011) with major ($M_W \geq 5.5$) historical (CPTI11, Rovida et al., 2011) and instrumental earthquakes (ISIDe database, Working Group INGV, 2015). (b) Intra-Apennine Quaternary extensional belt (light grey area) bounded by active and possibly seismogenic east-dipping (blue) and west-dipping (green) faults, with focal mechanisms of earthquakes from 1976 to 2014, with $M_w \geq 4.0$ and hypocentral depths <35 km (RCMT and TDMT database, available online at http://www.bo.ingv.it/RCMT/ and http://cnt.rm.ingv.it/tdmt.html, respectively); GPS data (blue arrows) are from D'Agostino et al. (2013) and refer to the stations CETR and PRAI on the Tyrrhenian coast. Rectangle represents the study area of Fig. 1c, 2, 8a and 9a. (c) Active faults from literature within the study area, with most significant historical and instrumental earthquakes. The yellow stars refer to the Pollino 2010–2014 seismic activity ($M_w \geq 4.0$) from ISIDe database, Working Group INGV, 2015. The red stars refer to the CPTI11 historical seismicity from Rovida et al., 2011 with the exception of the 1693 event derived from CFTI4Med Catalog (Guidoboni et al., 2007) and from Tertulliani and Cucci (2014), labelled in figure with G and TC respectively. The green star and dots refer to the Mercure 1998 seismic sequence as relocated in Brozzetti et al. (2009). Focal mechanisms of the events with $M_w \geq 4.5$ as in Fig. 1b. (For interpretation of the references to colour in this figure legend, the reader is referred to the web version of this article.)

considered as active in previous works, crop out along the North-eastern border of the Mercure Basin (Castello Seluci-Timpa della Manca Fault, CPST), and along the Southern slope of Mount Pollino massif (Pollino fault, POL, and Castrovillari fault, CAS). The CPST was

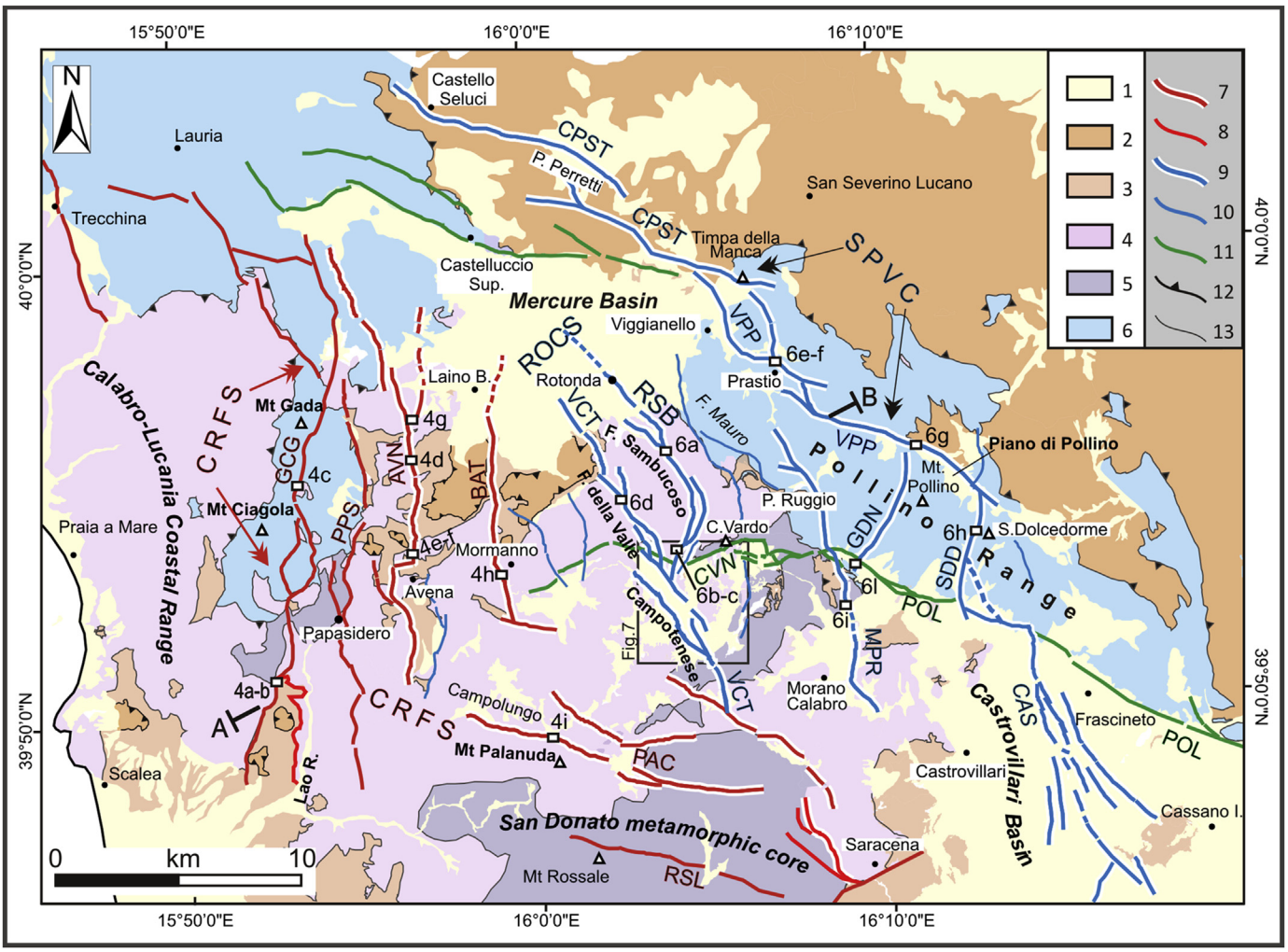

Fig. 2. Structural scheme of Quaternary and active faults in the Pollino area with the main tectonic units and the Quaternary basins (see Fig. 1b for the geographic location). The small white rectangle symbols, black rimmed with labels 4a-i and 6a-l indicate the locations of the faults-outcrops shown in the photographs of Fig. 3 and 5. Key: 1 = sin-extensional deposits of the continental basins (Mercure, Campotenese and Morano C. basins) and of the marine, evolving to continental, Castrovillari basin (Pleistocene-Holocene); 2 = allochthonous Liguride unit (mainly Late Cretaceous); 3 = "Scisti del Fiume Lao" *incertae sedis* Fm; 4 = Apennine Platform western unit (Verbicaro Unit, Late Triassic-Early Miocene); 5 = metalimestones and metapelites of the San Donato metamorphic core (Middle-Late Triassic?); 6 = Apennine Platform eastern Unit (Pollino unit, Late Triassic-Late Cretaceous); 7 = Middle Pleistocene to Holocene east-dipping normal fault; 8 = Early-Middle Pleistocene east-dipping normal fault; 9 = Late Pleistocene to Holocene west-dipping normal fault; 10 = Early-Middle Pleistocene west-dipping normal fault; 11 = Early to Middle Pleistocene south-dipping normal fault; 12 = thrust fault; 13 = basal contact of "Scisti del Fiume Lao" Fm. Acronyms as in Table 1: CRFS=Coastal Range Fault Set; ROCS = Rotonda-Campotenese Fault Set; SVPC= Castello Seluci-Viggianello-Piano di Pollino-Castrovillari Fault Set; MPR = Morano Calabro-Piano di Ruggio fault and GDN = Gaudolino fault; POL= Pollino fault; CVN= Cozzo Vardo-Cozzo Nisco fault. (For interpretation of the references to colour in this figure legend, the reader is referred to the web version of this article.)

interpreted by Brozzetti et al. (2009) as the seismogenic source of the Mercure 1998 earthquake (M_w 5.6) (Fig. 1c). The POL, based on the observation of bedrock scarps and paleo-seismological data, was interpreted as a 30 km-long active fault capable of surface faulting (Michetti et al., 1997), whose western segment was identified by Papanikolaou and Roberts (2007) in the ~ EW-striking Cozzo Vardo-Cozzo Nisco Fault (CVN in Figs. 1c and 2). Based on paleoseismological evidence, the CAS and the POL were associated to significant events (M 6.5–7.0) which occurred in 2000–410 B.C. and 500–900 A.D. (Michetti et al., 1997, 2000; Cinti et al., 1997, 2002). The epicenter of the 8 January 1693 earthquake is also located within the hanging wall block of the CAS. This event, which was first reported in the CFTI4Med Catalog (Guidoboni et al., 2007) with M_w 5.7, was recently relocated and its magnitude reduced to 5.2 (Tertulliani and Cucci, 2014). Two other significant M_w > 5.0 historical events located between the epicentres of the Mercure 1998 and the Mormanno 2012 earthquakes, are the earthquakes of 1894 (M_w 5.1) and 1708 (M_w 5.5) (Fig. 1c). All the major historical and instrumental earthquakes known near the area affected by the recent 2010–2014 Pollino seismic activity (e.g. the 1693, 1708, 1894 and 1998 earthquakes in Fig. 1c) are of moderate magnitude (M_w 5.1–5.6).

1.2. The reconstruction of the quaternary and active fault pattern

A structural analysis in an area of about 1200 km^2 along the Pollino range, and to the West was carried out (Fig. 2). The structural analysis was integrated through the systematic visual interpretation of a set of black-and-white stereoscopic aerial photographs flown in 1991 at a nominal scale of 1:33,000. Two interpreters performed the photo-interpretation (Supplementary data S1) using a Galileo SFG 3/b discussion stereoscope, with 1.25 × and 4 × zoom capabilities. Field surveys were subsequently executed to validate morpho-structural information. All the

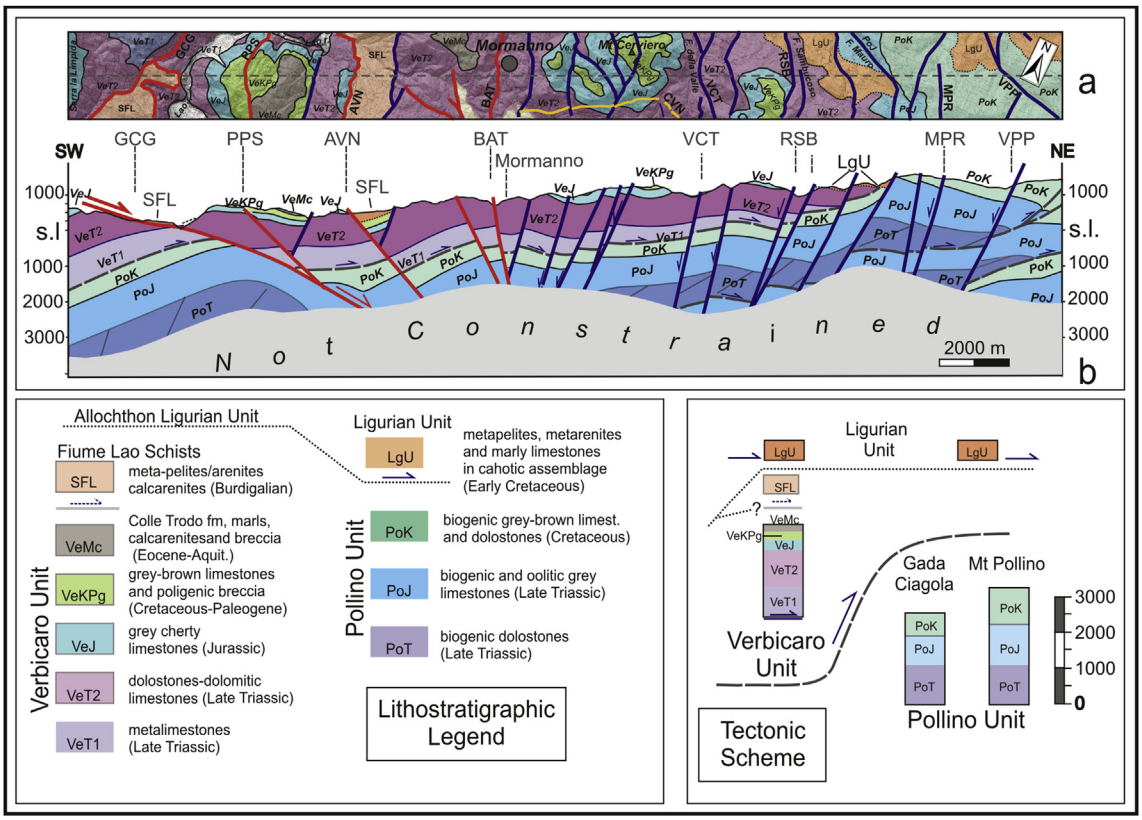

Fig. 3. a) Detailed geological map in a 2 km-wide strip centered in the section trace A-B of Fig. 2 and its interpretative section (b). Stratigraphy and thickness of the three major superimposed units (Ligurian allochthon = LGU, Verbicaro = Ve and Pollino = Po units) are reconstructed through literature data (Servizio Geologico d'Italia, 1970, 1971, 2011 Ghisetti and Vezzani, 1983; Iannace et al., 2004) integrated with original surveys; key: T1 = Middle-Late Triassic; T2 = Late Triassic; J = Jurassic; K= Cretaceous; Pg = Paleogene; Mc = Miocene. SFL = "Scisti del Fiume Lao Fm"; thick red and blue lines = east- and west-dipping Quaternary normal faults; thin grey dashed line = pre-existing thrust structure. (For interpretation of the references to colour in this figure legend, the reader is referred to the web version of this article.)

information collected was used to prepare a 1:25,000 scale map of Quaternary and active faults (See Supplementary data S2) schematized in Fig. 2. Moreover, a database of structural-kinematic data listing information collected at 114 survey sites was compiled (SS) (Fig. 5 and partially in the Supplementary data S3). Information regarding the main and/or most significant fault segments, including length, strike direction, dip-angle, rake, long-term and where possible, Late Pleistocene-Holocene displacement, time of activity, slip rate, and the fault acronym, are all listed in Table 1.

We recognized three main sets of genetically related normal and normal-oblique faults. One set consists of East- to NNE-dipping faults, and the other, two sets of SW-dipping faults (Fig. 2). The E/NNE-dipping set, referred to as the Coastal Range Fault Set (CRFS, Fig. 2), bounds to west the local portion of the Quaternary Extensional Belt (light blue domain in Fig. 1b). In the study area, the CRFS encompasses four sub-parallel fault alignments exhibiting mainly a North-South strike-direction (with dip-slip kinematics), alternating to WNW-ESE transfer segments (normal-dextral kinematics, with a significant strike-slip component). Their effective extent and surface geometry were largely unknown in past studies.

The SW-dipping faults are arranged in two main NW-SE-striking sets referred to as "Western" and "Eastern" sets. Other isolated Quaternary faults were mapped in the intermediate sector between the two main SW-dipping sets (Fig. 2).

The SW-dipping Western set, ie, the Rotonda – Campotenese set - ROCS (Fig. 2) extends across the 2010–2014 Pollino epicentral area and consists of two main right-stepping en echelon fault segments (RSB and VCT in Fig. 2). The Eastern SW-dipping set i.e. the Seluci - Viggianello – Piano di Pollino – Castrovillari fault (SVPC, Fig. 2), represents the front of the Quaternary extensional belt, i.e., the W-dipping break-away fault, and consists of three main en echelon faults ranging in strike from WNW-ESE to NNW-SSE (from the North to the South, the CPST, VPP and CAS faults).

In the intermediate region between the ROCS and the SVPC sets, W to NW-dipping faults, the Morano Calabro – Piano di Ruggio (MPR) fault and the Gaudolino (GDN) fault show evidence of Late Quaternary activity (Fig. 2).

In the following, additional details on the geometry, the kinematics, and the timing of the main extensional faults, with emphasis on the faults located close to the 2010–2014 Pollino epicentral area are given.

After defining the fault pattern, the geological displacement value associate to each fault along a regional geological section crossing nearly orthogonal the major structures was estimated (Fig. 3). The section crosses an area characterized by continuous and good quality bedrock exposure, where, with an accurate survey, we carefully constrained the stratigraphy of the displaced units and elaborated a detailed geological map in a 2 km-wide strip centered in the section trace (Fig. 3a).

The stratigraphy was primarily derived from published maps and subsequently refined in the field. Among previously used maps, the following are particularly worthy noting: i) 1:100.000 scale, 210-Verbicaro Sheet of the Carta Geologica d'Italia (Servizio Geologico d'Italia, 1970), ii) 1:100.000 Iannace et al. (2004) map of the Maratea-Castrovillari area and, iii) 1:50.000 scale Ghisetti and Vezzani (1983) Structural Map of Mount Pollino.

Table 1
Length, strike, dip-angle, associate displacement, age of activity and throw-rates of Quaternary active faults in the study area. One asterisk near the fault acronym indicates the newly identified faults; two asterisks indicate previously mapped faults that are significantly extended or modified in this work, faults without asterisk are active faults from the literature.

Fault Sys.	Fault name/ *Segment name*	Acronym	Length km	Strike direction	Dip angle	Rake	Displac. Along-Dip. m	Heave m	Throw m	Age of activity	Throw Rate (mm/y)	Notes and constraints on age of activity
CRFS	Gada - Ciagola	CGC**	28	N010 N160	18 –25° E	85	2580	2440	840	Early-Mid. Pleist.	–	Displacement of ancient till deposits (Early-lower Middle Pleistocene?; no stratigraphic and morpho-structural evidence of recent activity
CRFS	Papasidero	PPS*	24	N010 N170	30 –45° E	85	190	140	140	Early-Mid. Pleist.	–	Lack of clear stratigraphic and morpho-structural evidence o recent activity
CRFS	Avena	AVN*	20	N010 N180	50 –60° E	90	680	440	520	Middle - Late Pleist. (Holocene?)	0.70	Displacement of alluvial fan conglomerates of the western Mercure basin fill (Middle Galerian, Isernia F.U.~736kyr); marked control on Lao r. hydrographic network
CRFS	Battendiero	BAT*	11	N010 N150	70 –80° E	–	160	40	150	Middle - Late Pleist. (Holocene?)	0.35	Influence on talweg of Battendiero r. (De Martini, 1996); offset of lacustrine deposits of Mercure basin; displacement of recent slope debris (Late Pleist.?);
CRFS	Palanuda Mount	PAC*	13	N085 N110	50 –70° NNE	88	–	–	–	Middle - Late Pleist.	–	Free face with hectometric continuity and 1- 2 m-high scarp in fault breccia, along north slope of Mt Palanuda
CRFS	Rossale	RSL*	10	N100	50 –70° NNE	–	–	–	–	Early-Mid. Pleist.	–	–
ROCS	Fosso della Valle -Campotenese	VCT**	15	N160	60 –80° W	90	120	30	120	Uppermost Middle Pleist. - Holocene	0.30	Offset of the top surface of Mercure deposits (post-440kyr according to Giaccio et al., 2014); dissection of CVN fault (dated at Middle Pleistocene by Schiattarella et al., 1994); very recent subsidence of Campotenese basin
ROCS	Rotonda - Sambucoso	RSB**	10	N170 N190	60 –70° W	78 82	230	80	210	Uppermost Middle Pleist. - Holocene	0.50	See previous note
SVPC	Castello Seluci - Timpa d. Manca/ *Castello Seluci Piana Perretti*	CSPT	11	N120	55 –70° SSW	80	–	–	–	Late Pleistocene - Holocene*	–	*Seismogenic source of the 1998, Mw 5.6 Mercure earthquake according to Brozzetti et al., 2009
SVPC	Castello Seluci - Timpa d. Manca/ *La Fagosa - Timpa d. Manca*	CSPT	12.5	N120	55 –70° SSW	80	–	–	–	Late Pleistocene - Holocene*	–	*Seismogenic source of the 1998, Mw 5.6 Mercure earthquake according to Brozzetti et al., 2009
SVPC	Viggianello -Piano di Pollino/ Viggianello-Prastio	VPP**	6	N120	55 –70° SSW	90	–	–	–	Uppermost Middle Pleistocene - Holocene (?)	0.20 0.40	Fault scarp displacing the ~18 kyr (L.G.M.) slope, with 3.5–8 m associated throw
SVPC	Viggianello -Piano di Pollino/ Vacquaro - Piano Pollino	VPP**	10	N120	55 –70° SSW	–	230	100	200	Uppermost Middle Pleistocene - Holocene (?)	–	Physical Continuity with the VPP
SVPC	Serra Dolcedorme	SDD*	5	N170	65 –80° W	–	50–100	20–40	50 –100	Late Pleistocene - Holocene (?)	–	5 m-high free-face displacing present topography along the Serra Dolcedorme Mt crest; Near-continuity with Castrovillari fault
Other Fault	Castrovillari	CAS	13	N160	60 –80° WSW	85	–	–	**100 –150	Late Pleistocene - Holocene	1**	**Cinti et al., 2002
Other Fault	Morano C. – Piano di Ruggio	MPR*	12.5	N160	60-70° WSW	91	80	20	80	Middle - Late Pleistocene (Holocene?)	–	Proposed as seismogenic source of the 2011, Mw 4.3 Morano C. earthq., this paper
Other Fault	Gaudolino	GDN**	6	N40 N180	60 –70° W	90	210	70	200	Middle - Late Pleistocene (Holocene?)	0.15	1.5 m- high scarp offsetting present topography with associated wedge of dark-brown colluvium (Holocene?)

Where both the estimates of the geological displacement and the timing of the faults are available, the long-term slip rate of the active faults is provided. Table 1 summarizes all the up-to-date data concerning the studied Quaternary and active faults.

1.3. E-dipping Coastal Range Fault Set (CRFS)

The CRFS consists of four main N-S-striking, E-dipping normal fault segments including, the Gada – Ciagola (GCG), the Papasidero (PPS), the Avena (AVN), and the Battendiero (BAT) faults from West

to East (Fig. 2). To the S, the PPS and the AVN faults are in close continuity with the NNE-dipping Rossale (RSL) and Palanuda – Campolungo (PAC) faults. On the surface, the CRFS faults displace the Mesozoic-Cenozoic succession of the Verbicaro and Pollino Units that, along the GCG and the AVN faults, come into contact with the metapelitic "Scisti del F. Lao" fm. The latter is a matter of debate and is considered by Iannace et al. (2004) as the effective stratigraphic top of the Verbicaro Unit whereas, by the recent 542 sheet of the Carta Geologica d'Italia (Servizio Geologico d'Italia, 2011; Ietto and Ietto, 2011), as belonging to the allochthon (Frido Fm, See Tectono-Stratigraphic Scheme in Fig. 3). Whatever its paleo-geographic attribution, its position in the tectonic pile (at the top of the Verbicaro unit) is well defined and permits reliable assessment of the displacement associated to the CRFS faults.

In the field, the dip-angles measured on the various CRFS faults (Table 1) increase from West to East. They are in the range of 18°–25°on the GCG fault (Figs. 3b and 4a–c), between 30° and 45° on the PPS fault, between 50° and 60° along the AVN fault (Figs. 3b and 4d–g), and varies between 70° and 80° on the BAT fault (Figs. 3b and 4h). Conversely, the maximum estimated geological displacement, (measured along the fault dip) decreases from West to East, going from ~2800 m for the GCG and the PPS faults (the PPS is a shallow splay of the GCG), to ~700 m for the AVN fault, to only 160 m for the BAT fault (Fig. 3b, Table 1).

Field data reveals that the GCG fault is the major structure of the CRFS, with an average dip-angle of ~20°. Therefore, from a geometrical point of view, it can be defined as a low-angle Normal Fault (LANF, Fig. 4a–c and 5, SS1 and SS3). Good quality fault-slip data obtained along the GCG and the AVN faults (Fig. 5, SS1–SS16) are indicative of extensional kinematics, with prevailingly dip-slip or slightly oblique-slip movements, coherent with a sub-horizontal and nearly E-W extension. This is confirmed in Fig. 5 by the contour diagram of the geological T-axes averaged along the entire striated CRFS fault planes (E-dip/T-Axes, computed through Bingham statistics, Bingham, 1974).

As regards to the age of faulting, along the GCG and the PPS faults (the westernmost CRFS faults), the only significant observation is represented by a faulted slope breccia, of an unspecified Pleistocene age (Servizio Geologico d'Italia, 1970), displaced nearly 1,5 South of Mount Gada (GCG fault, Fig. 4c, SS1). This breccia is eroded and elevated with respect to the valley floor and is unrelated to the evolution of the present slope. This evidence suggests that its deposition occurred before the Middle Pleistocene but no persuasive data are available on the age of its faulting.

In fact, along the GCG and PPS, the general scarcity of very recent deposits preclude clear evidence of Late Pleistocene activity.

An Early to Middle Pleistocene age of activity would also be coherent with the timing suggested by Robustelli et al. (2014) based on the displacement of the topographic paleo-surfaces recognized regionally in the Lao valley, and also extending to the summit of Mount Ciagola.

Differently, the AVN and the BAT faults show a "fresh" geomorphic signature, including kilometric-scale straight slopes, faceted spurs, and well-preserved scarps. The two faults also control the river network, locally (Figs. 2 and 4d-f and h). The Northern segment of the AVN cuts the alluvial fan conglomerates of the Western Mercure basin fill (Fig. 4g) whose deposition was attributed to the Middle Pleistocene by Cavinato et al. (2001) based on the age of Middle Galerian mammals, and to the interval 700-550 kyr by Giaccio et al. (2014) based on tephro-chronological analyses. The latter data implies an age of activity for the AVN fault, post-dating the lower part of the Middle Pleistocene and provide an assessment of the long-term slip-rate of the fault (Table 1).

On the contrary, with reference to the BAT fault, evidence of offset on poorly cemented debris, in equilibrium with the present slope of the Battendiero Valley (Fig. 4h), could be related to fault activity lasting until the Late Pleistocene, or even in more recent periods.

Summarising, based on the available stratigraphic and morpho-structural data, we hypothesize that the GCG fault represents the earlier fault of the CRFS (Early-Middle Pleistocene in age), whereas a recent origin and evolution could have characterized the two easternmost faults i.e. the AVN fault and the BAT fault with their NNE-dipping prolongations (e.g. the PAC fault, Figs. 2 and 4i), whose activity started during the Middle-Late Pleistocene, and is possibly still on-going.

Overall, the CRFS evolved following a West to East younging trend that sounds coherent with the Eastward decrease of the geological displacement associated to the single faults (Fig. 3, Table 1).

1.4. Western west-dipping set

The Rotonda – Campotenese Set (ROCS) is a right-stepping en echelon set of anastomosed fault segments developed for a total length of 15 km with an average N160°direction, from the Southern side of the Mercure basin to the village of Campotenese (Fig. 2). Two main faults can be recognized in this set: the Rotonda – Sambucoso (RSB) fault, and the Fosso della Valle – Campotenese (VCT) fault (Fig. 2). The RSB fault extends for nearly 10 km, striking from NNW-SSE to N-S. At the surface, along the section of Fig. 3, this fault cuts the Eastern edge of the Verbicaro Unit, characterized by dolostones (Triassic in age) and cherty limestone (Jurassic in age, Ghisetti and Vezzani, 1983; Servizio Geologico d'Italia, 1971). The maximum dip parallel to geological displacement of the RSB fault is ~500 m (Table 1), estimated cumulating the displacement caused by two closely-spaced splay faults (Figs. 2 and 3). Good exposures of the RSB fault plane were observed West of Cozzo Vardo and along the East side of Sambucoso River valley (Fig. 6a–c) where the fault cuts the slope debris referred to Late Pleistocene-Holocene (Servizio Geologico d'Italia, 1971) with normal and normal-oblique kinematics (SS33, SS34, SS38, SS39 in Fig. 5).

The VCT faults extends in the NW-SE direction (N155°) for ~15 km from the border of the Mercure basin to the SW boundary of the Campotenese Basin. Along the Fosso della Valle, the VCT faults down throws by ~120 m the Triassic-Jurassic stratigraphic boundary (Fig. 3a) and within the footwall, the Triassic dolostones are involved in a wide damage zone characterized by tens of meters of fault breccia and by closely-spaced meso-faults (Fig. 6d) with a prevailing dip-slip kinematics (Fig. 5, SS29, SS31, SS32, SS35). Close to the Northern tip point, the geological expression of the fault gradually becomes weaker. An evident and continuous scarp, 3 km long, carved on the present topography, marks its trace within the Mercure basin. Southward, the VCT is buried below the Holocene alluvial deposits, but its continuation can be clearly detected based on its control on the thickness of the deposits filling the Campotenese plain (Fig. 7). The fault in fact, subdivides the depression in a Western sector (VCT hanging wall) where the Pleistocene-Holocene deposits display the maximum thickness and are drilled for at least 30 m (Fig. 7, including wells stratigraphy and sections on the left), and an Eastern one (VCT footwall), where some terraced Middle Pleistocene silts and sands (Schiattarella et al., 1994) and slight coatings (generally < 2 m thick) of Late Pleistocene colluvium crop out.

Further indirect evidence of the Late Quaternary activity of the RSB and VCT faults comes from their cross-cut relationships with the Cozzo Vardo-Cozzo Nisco fault (CVN, Figs. 2 and 7., Fig. 5, SS 42–46) whose age is attributed to the Middle Pleistocene by Schiattarella et al. (1994) and suggested, without strict constraints, as Late Pleistocene age by Papanikolaou and Roberts (2007).

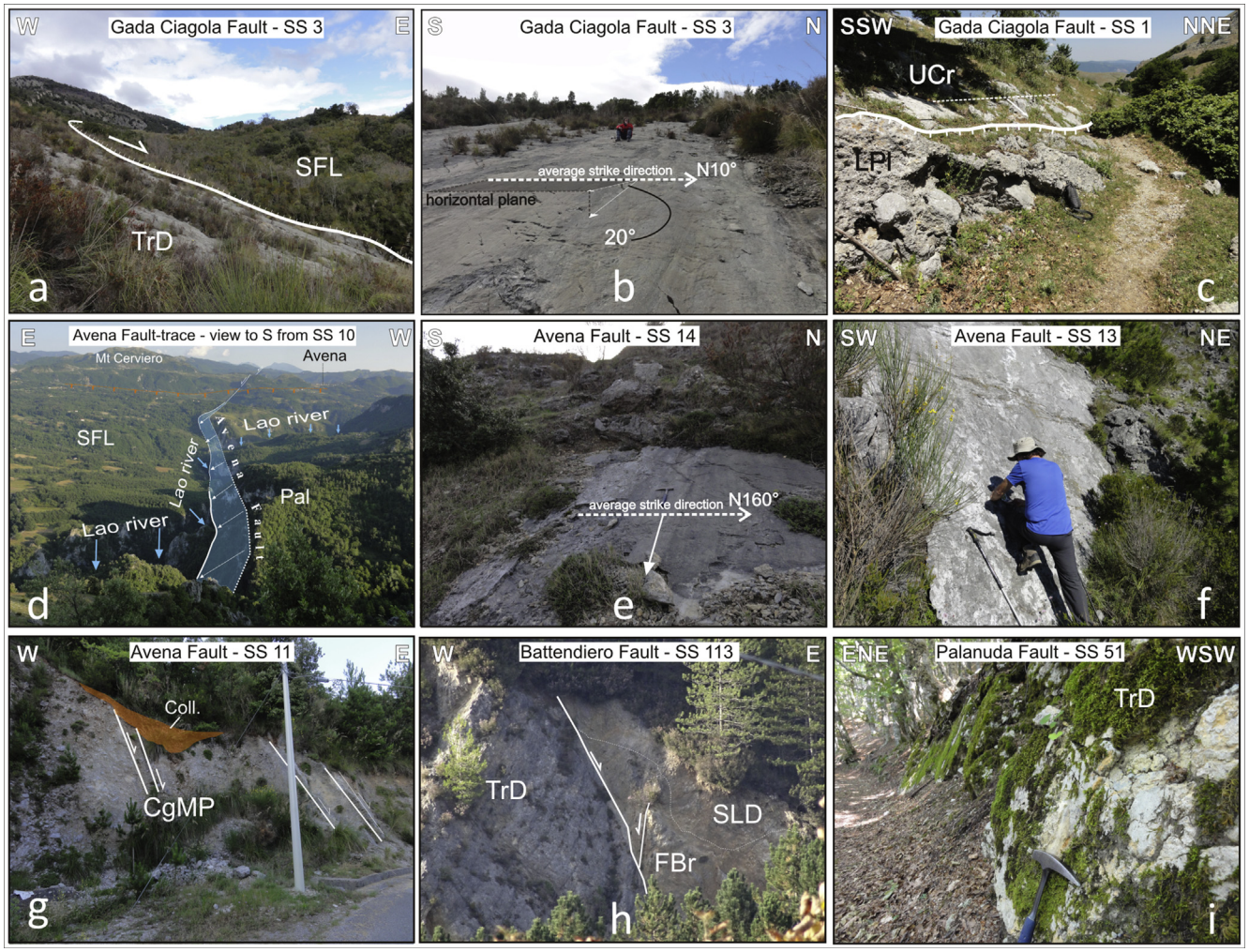

Fig. 4. Outcrop views of the east-dipping Quaternary normal fault belonging to the CRFS (locations in Fig. 2 as small black rectangles); (a), (b), (c) = spectacular hectometric-scale fault plane and details of kinematic indicators from the Gada-Ciagola LANF (GCG; TrD = Triassic Verbicaro dolostones, SFL= Scisti del Fiume Lao Fm; LPL = lower Pleistocene breccia); (d) = trace of the AVN fault east of Mt Ciagola, showing the control on the local drainage network of the Lao river, Pal = Paleocene carbonates, SFL= Scisti del Fiume Lao Fm; (e), (f) = fault mirrors along the AVN trace; (g) = northern strand of the AVN displacing the Middle Pleistocene conglomerates of the Mercure basin fill (CgMP); an unconformable dark-brown westward-thickening colluvial deposit (Coll) of uncertain age (Late Pleistocene-Holocene?) is associated to the fault zone; (h) = fault plane with associated sheared breccia on the BAT fault (TrD = Triassic dolostones, FBr=Fault breccia, SLD= Slope debris); (i) = NNE-dipping fault-scarp along the Palanuda-Campolungo fault (PAC). An uninterpreted version of this same figure, reporting the coordinates of the photographed sites, is also provided in the Supplementary data S4. (For interpretation of the references to colour in this figure legend, the reader is referred to the web version of this article.)

A detailed structural survey performed on the interaction zone between the CVN, the RSB and the VCT, highlighted the fact that these two latter faults dissect the former (Fig. 7).

Taking into account these relationships and the control that the RSB and VCT exerts on the setting of the Campotenese basin, the onset of their activity can be placed during the Middle Pleistocene. These same observations lead to exclude the Late Pleistocene activity of the CVN.

1.5. Eastern west-dipping set

The Eastern west-dipping fault set (SVPC, Fig. 2), includes, three major faults from NW to SE: Castello Seluci-Piana Perretti-Timpa della Manca (CPST), Viggianello-Piano di Pollino (VPP) and Castrovillari faults (CAS).

The CPST consists of two distinct en echelon segments, both striking, on average, N120°-125° and dipping 50°–70° to the SSW (Fig. 2). Reference is made to Brozzetti et al. (2009) recent paper, giving detailed geometrical and kinematic descriptions of this fault which the authors consider the seismogenic source of the 1998, M_w5.6 Mercure Earthquake.

Prior to this study, the VPP was mapped only in the Viggianello-Prastio area. We mapped it far to the South, along an extent of 16 km along-strike, mainly in N120° direction, with local deviations to NNW-SSE (Fig. 2). Its best exposure occurs near the Prastio Village (Fig. 6e, f) where this fault, dipping 55° Southwest, displaces the debris mantling the present slope with nearly dip-slip kinematics and with estimated throw varying from 3.5 m to 8 m (Fig. 5, SS 17–19 and Fig. 6f). This deposit, consisting of a poorly cemented calcareous breccia in abundant brown-reddish matrix, due to its scarce remodelling and its position along the foot of the slope, can be dated back to the Late Pleistocene age. In analogy with a number of papers (Roberts and Michetti, 2004; Papanikolaou et al., 2005; Papanikolaou and Roberts, 2007; among others), we believe that the slope, displaced by the VPP, formed and regularized during the Last Glacial Maximum (LGM), at ~18 kyr. According to this assumption, the measured post-LGM displacement allows a preliminary assessment of the Late Quaternary slip-rate across this

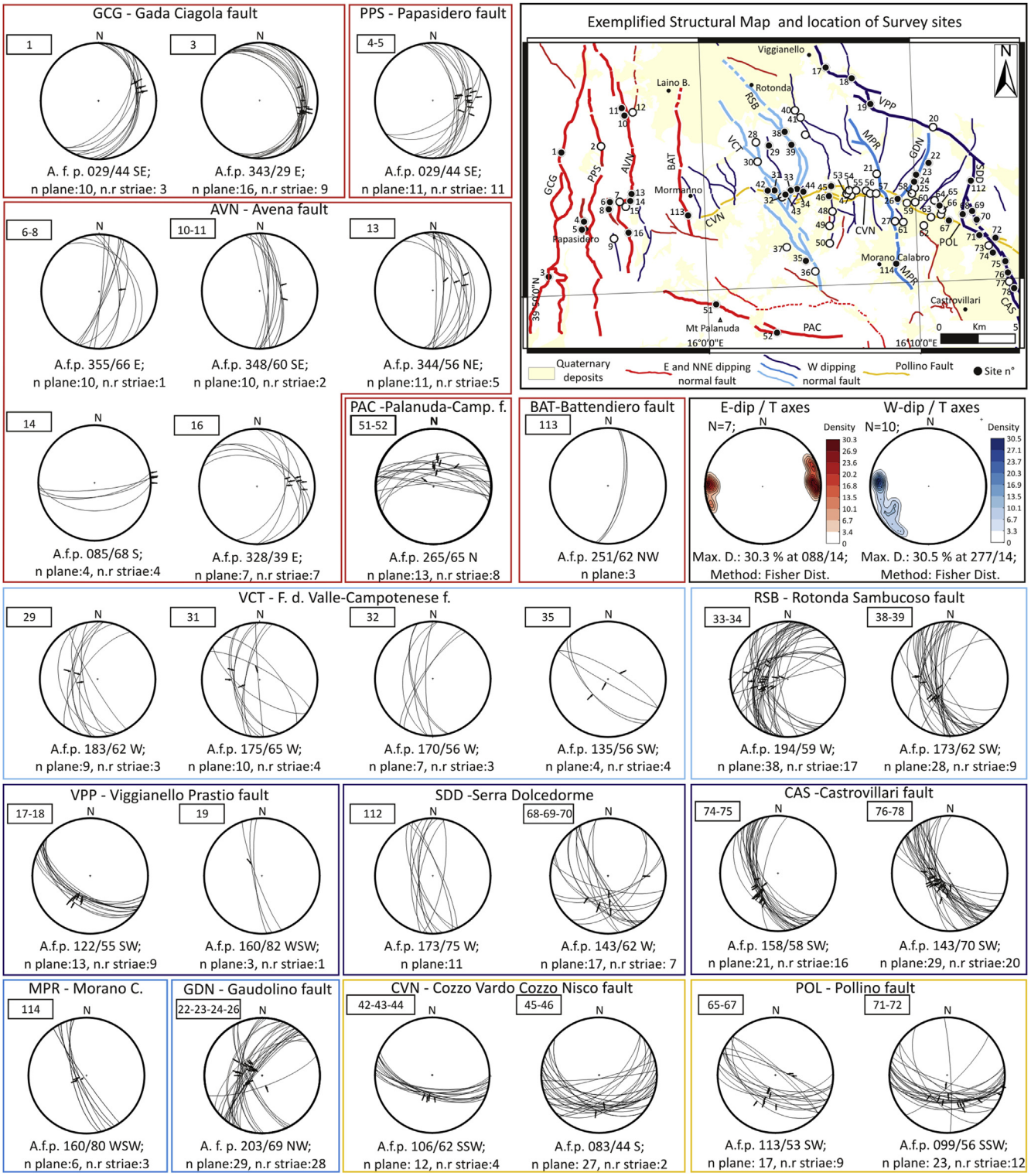

Fig. 5. Structural analysis carried out on the Quaternary faults of the Mercure-Pollino area; the map (top right) shows the location of the survey sites (SS) that are structurally-homogeneous outcrops, or group of close outcrops, at a maximum distance of 500 m from each other and falling within the diameter of each small black circle on the map. Acronyms are the same of Table 1 and Fig. 2). The number in rectangle, at the top-left of each plot, refers to the structural site, or group of sites reported in the location map and in the text. A.f.p. = attitude of the average fault plane. The two contour diagrams below the structural sketch, show the density distribution of the extension axes obtained from the striated planes belonging to the east-dipping (E-dip/T-Axes) and west-dipping (W-dip/T-Axes) fault sets. White circles mark the locations of additional survey sites on secondary structures whose structural data are provided as Supplementary data S3. (For interpretation of the references to colour in this figure legend, the reader is referred to the web version of this article.)

fault in 0.2–0.4 mm/yr (Table 1).

To the South, the VPP extends for at least another 10 km, delimiting to North-East the Piano di Pollino Holocene depression (Fig. 2 and 6g), and connects to a N-S-striking, W-dipping, fault that

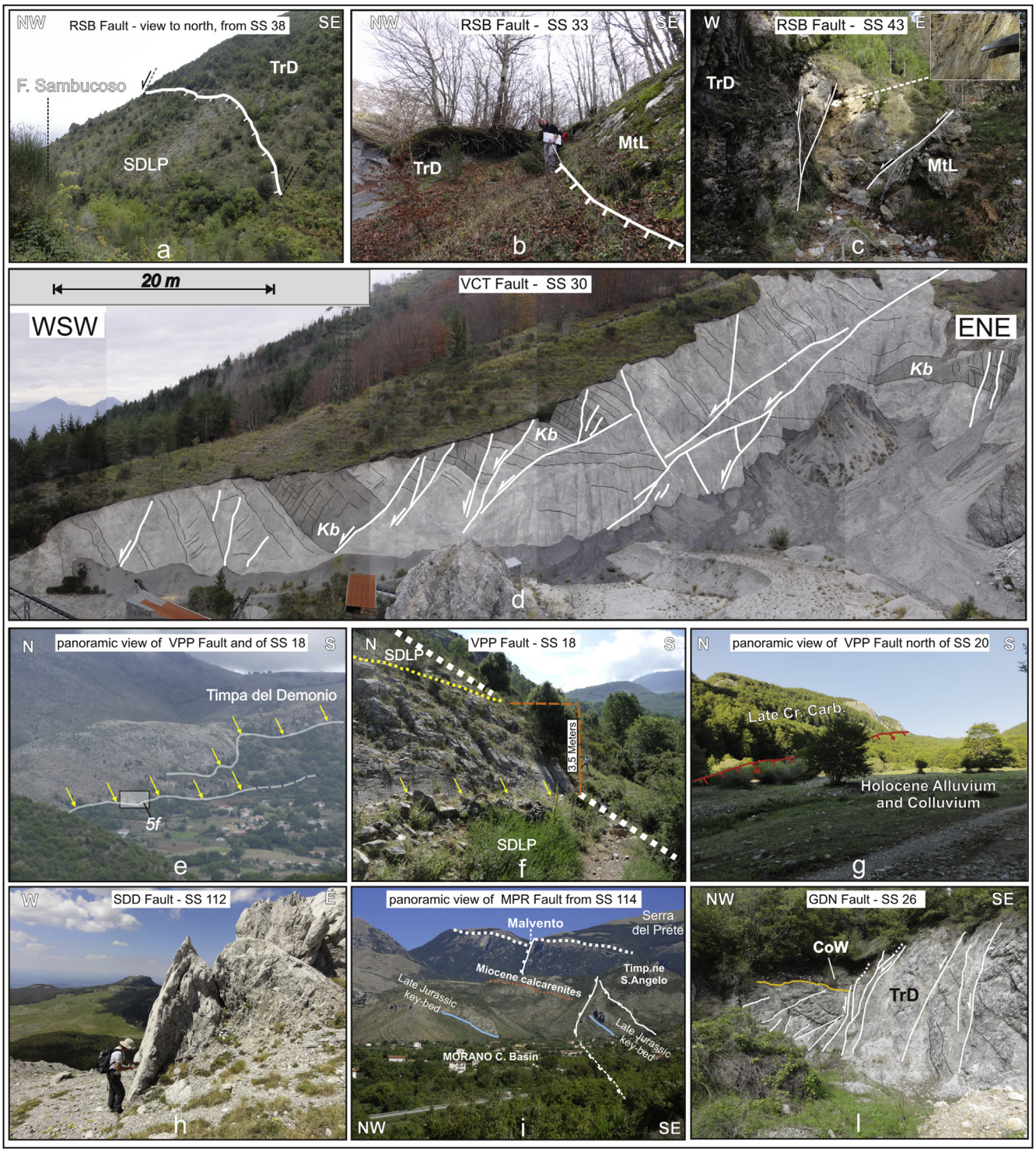

Fig. 6. Outcrop views of the west-dipping Quaternary normal faults detected in the study area (locations in Fig. 2 as small black rectangles). (a): continuous fault scarps along the Rotonda-Sambucoso fault, between the Triassic dolostones (TrD) and the Late Pleistocene slope-debris (SDLP); (b)–(c): RSB normal fault plane and the associate damage zone, west of Cozzo Vardo; the inset in the top right shows the nearly dip-slip normal striations on the fault plane (MtL = Middle-Late Triassic meta-limestones, TrD = Late Triassic dolostones); (d): dolostone quarry along the road Rotonda-Campotenese, a penetrative set of SW-dipping normal faults gives rise, within the VCT fault-zone, to an eastward-tilted domino-like structure; (e): panoramic view of the VPP fault, consisting of two closely spaced, en echelon segments both marked by a continuous slope-break; the black rectangle shows the location of the outcrop of Fig. 5f; (f): the VPP fault near Prastio; the yellow dotted line marks the unconformable contact between the calcareous bedrock and the Late Pleistocene slope debris (SDLP) displaced by the fault; (g): fault–related slope along the VPP in the Vacquarro valley 3 km WNW of Piano di Pollino (view to SE); (h): free face of the SDD fault displacing the crest-line of Serra Dolcedorme; (i): panoramic view (to north) of the MPR fault with displaced key beds and other stratigraphic layers; (l): outcrop of the Gaudolino Fault along the north side of Valle della Casotta; TrD = Triassic dolostones; Coll = colluvium consisting of very coarse grained pebbles and boulders in a dark-brown soil matrix, showing a clear growth geometry towards the fault. An uninterpreted version of this same figure, reporting the coordinates of the photographed sites, is also provided in the Supporting material S5. (For interpretation of the references to colour in this figure legend, the reader is referred to the web version of this article.)

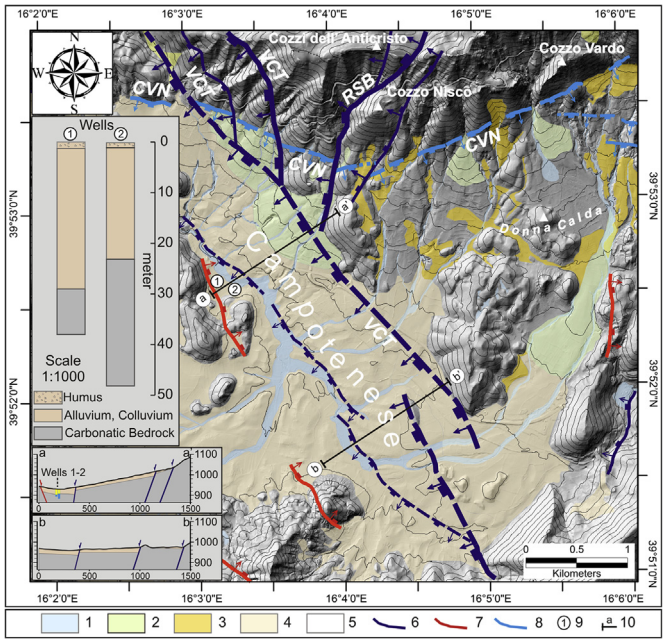

Fig. 7. Detail of the Campotenese area showing a survey of the Quaternary units and the cut-off relationships between the W- to SW-dipping normal faults of the ROCS (RSB and VCT faults, dark-blue lines) and the South-dipping Cozzo Vardo-Cozzo Nisco Fault (CVN, light-blue line). The insets on the left, show the schematic stratigraphy of two available boreholes in the Campotenese Plain (above) and two shallow geological sections across the basin, drawn along the traces a-a' and b-b'(vertical exaggeration 2×). Key: 1 = Holocene alluvium of the present floodplain of the Battendiero river; 2 = Late Pleistocene-Holocene alluvial fans and colluvium; 3 = Late Pleistocene slope debris; 4 = Middle to Late Pleistocene fill of the Campotenese basin (mainly lacustrine); 5 = undifferentiated bedrock; 6 = west-dipping normal fault (dotted line where buried); 7 = east-dipping normal fault; 8 = trace of the south-dipping Cozzo Vardo-Cozzo Nisco fault (CVN); 9 = borehole location; 10 = trace of geological section. (For interpretation of the references to colour in this figure legend, the reader is referred to the web version of this article.)

offsets the crest-line of Serra Dolcedorme with a fresh fault scarp (Serra Dolcedorme fault, SDD in Fig. 6h and SS 112 in Fig. 5). Further South, this fault was surveyed for nearly 4 km developing in left-stepping en echelon arrangement with the Castrovillari fault (CAS, Fig. 2).

The zone of interaction between the SDD the POL and the CAS is unfortunately badly exposed and complicated by scattered bedrock outcrops, belonging to different tectonic units. It is interpreted in alternative ways by the various authors that studied these faults (Ghisetti and Vezzani, 1982; Cinti et al., 1997, 2002; Michetti et al., 1997, 2000; Ercoli et al., 2013).

Our geological and morpho-structural mapping highlighted that in correspondence of the intersection between the SDD and the POL, the latter shows an offset of some hundreds of meters (Fig. 2) suggesting, that the SDD cuts and displaces the POL and represents "de facto", the northern prosecution of the CAS.

This possible link between the SDD and the CAS, crossing, or locally reactivating a portion of the POL is also supported by the widespread evidence of NW-SE-striking mesoscopic normal faults in the zone of interaction between these faults (Fig. 5, SS 68–70).

The CAS is probably the best-known active fault of Northern Calabria, along where the occurrence of repeated seismic events during the past 30–40 Kyr (Cinti et al., 2002) is accepted, based on paleo-seismological data (Michetti et al., 1997; Cinti et al., 1997, 2002). Its fault trace consists of several sub-parallel segments in a N160°average direction, gradually rotating to N120° approaching the POL. Our structural analysis along the CAS fault-scarps displacing the Late Pleistocene age deposits (in the main N160° segment) confirms its normal kinematics (SS74-SS78 in Fig. 5).

1.6. Other west-dipping Late Quaternary faults

The area between the ROCS and the SVPC is crossed by at least two other faults i.e., the Morano Calabro – Piano di Ruggio (MPR) fault, and the Gaudolino (GDN) fault, both showing evidence of recent activity. The extent and continuity of the faults are poorly constrained, due to abundant alluvial and slope debris cover. Nevertheless, they could be significant from a seismotectonic point of view, because they crop out close to the Pollino epicentral area. Through the integration of field data and photo-geological interpretation, locally integrated with the visual analysis of 1 m-resolution images, derived from Lidar Survey (available online as Web Map Services at http://www.pcn.minambiente.it/GN/), the MPR was followed for ~ 12,5 km along strike. Where exposed, the MPR dips westward at a high-angle of 60–70°, with dip-slip kinematics. It juxtaposes the Jurassic-Cretaceous carbonates of the Verbicaro Unit (footwall) with the Paleocene-Miocene calcarenites resting uncomfortably above them (hanging wall) (Servizio Geologico d'Italia, 1971; Ghisetti and Vezzani, 1983), with a minimum estimated throw of ~80 m (Timpone S. Angelo area). Higher values of throw could reasonably be associated to the Southernmost sector, where the fault borders the Morano Calabro Pleistocene basin (Fig. 5, SS 114 and Fig. 6i). The present activity of the MPR can be inferred by indirect evidence as the location of Pleistocene-Holocene intra-mountain depressions along the fault trace (Piano di Ruggio, Morano Basin, Fig. 2) and the influence that it exerts on the topography.

The GDN belongs to a minor, but well evident, set of NNE-SSW-striking structures nearly orthogonal to the Pollino ridge showing normal kinematics (Fig. 2). The most convincing evidence of GDN activity comes from the faulting of very recent slope debris and colluvium along the Southern side of the Gaudolino valley in the site shown as 6l in Fig. 2. In the latter site, a N30°-striking, NW-dipping, fault (Fig. 5, SS22–SS26) offsets the Triassic dolostones in the bedrock (Ghisetti and Vezzani, 1983) and an overlying dark-brown colluvial deposit, grading upwards to the present soil, probably of Holocene age (Fig. 6l). The colluvium is sheared close to the fault plane and displays a wedge-shape geometry that is coherent with the growth above a downthrown hanging wall. Near the same locality, it was also possible to ascertain, with a detailed 1:5000 scale survey, that the trace of the POL undergoes a right-lateral offset in correspondence to the GDN fault (Fig. 2).

The W-dip/T-Axes contour diagram, shown in Fig. 5 illustrates the attitudes of the geological T-axes computed from the whole striated fault planes belonging to all the major west-dipping quaternary faults (ROCS, SVPC, MPR and GDN). The obtained values of the average WSW-ENE to W-E trending T-Axis are coherent with those obtained from the CRFS faults (E-dip/T-Axes) confirming that the East- and West-dipping sets are genetically linked and generated in response to the same regional stress field.

1.7. The 2010–2014 seismic activity

On 25 October 2012, at 23:05:24 (UTC), the study area was hit by an earthquake of magnitude M_W5.2 (M_L5.0, I_{max} IV EMS) (ISIDe database, Working Group INGV, 2015; D'Amico and Scarfì, 2012). This earthquake, which occurred nearly 70 km NNW from the town of Cosenza, close to the Mormanno locality on the Western side of Mount Pollino range, was the largest event of a long-lasting normal-faulting seismic activity, which mostly occurred from October 2010 to the beginning of 2013, and with another period of

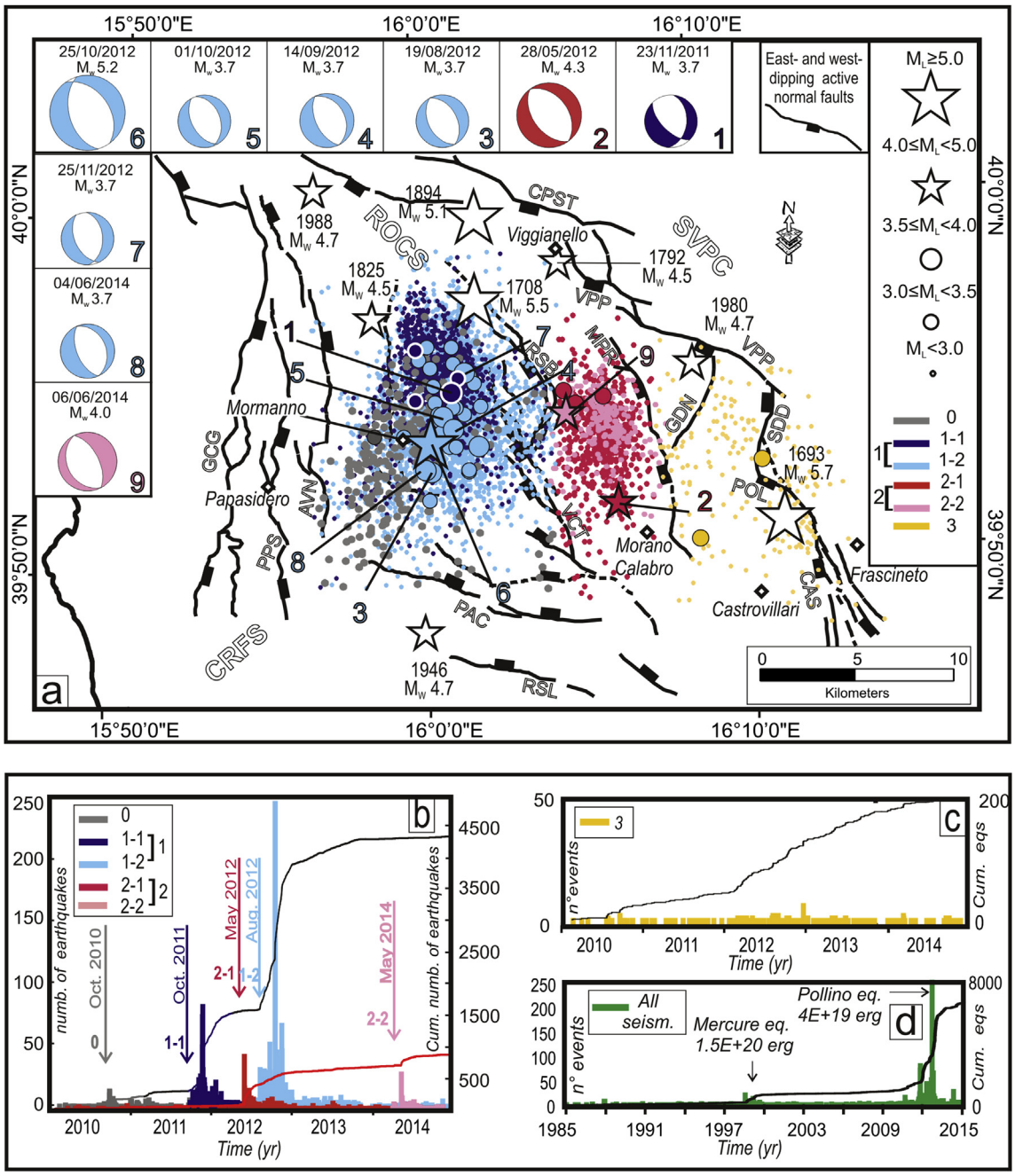

Fig. 8. Time-space evolution and focal mechanisms of the Pollino 2010–2014 seismic activity. (a) Epicentral distribution of events with local magnitude $0.1 \leq M_L \leq 5.0$, occurred from January 2010 to the end of December 2014 within the study area, as reported from ISIDe database, Working Group INGV (2015). The epicenter color code highlights earthquake clusters (grey, blue, light blue and red) and the background seismicity (yellow) as identified on the basis of the spatial distribution (cluster 0, 1, 2 and 3 moving from west to east) and temporal (0, 1-1, 1–2, 2, 3) evolution of the seismic sequence as subdivided in Fig. 8b and c. Focal mechanisms (1–9) of the most significant events of the seismic activity are from Totaro et al. (2015). The white stars represent the major historical and instrumental earthquakes from CPTI11 database (Rovida et al., 2011). (b) Daily event distribution and cumulative number of events referred to cluster 0 (grey histogram), cluster 1 (1-1 blue; 1–2 light blue histograms) and cluster 2 (red histogram). The arrows indicate the start date of the sub-sequences.(c) Daily event distribution and the cumulative number of events referred to the background seismicity (3). (d) Daily event distribution and the cumulative number of events occurred within the study area from 1985 to 2014 extracted from Italian Seismic Catalogue CSI (Castello et al., 2006), Italian Seismic Bulletin (2002–2005) and ISIDe database, Working Group INGV, 2015 (2005–2013). (For interpretation of the references to colour in this figure legend, the reader is referred to the web version of this article.)

accelerated seismic release in June 2014 (Fig. 8). Also taking into account the substantial improvement of the seismic network, it is possible to state that this sequence determined a significant increase in seismic activity, in an area characterized by low seismicity rate in instrumental times (from 1981 to 2009), with the exception of the 1998 Mercure seismic sequence (Fig. 8d).

The time-space analysis of the 2010–2014 seismicity highlights the fact that earthquakes are concentrated, from West to East, in three major, nearly N-S trending, clusters (0, 1 and 2) and in a more external minor one (cluster 3) (Fig. 8a). Spatially, cluster 0 partially overlaps cluster 1, while clusters 2 is well separated from the others.

Cluster 0 is elongated in direction NNE-SSW and concentrated to the West and South-West of cluster 1. This cluster, which is

confined westward by the Easternmost segment of the East-dipping CRFS, represents the earliest and westernmost activity (Fig. 8a, b) characterized by low magnitude events 0.3 ≤M_L ≤ 2.9.

Cluster 1 (blue and light blue symbols in Fig. 8), named the Mormanno cluster, is the major one in terms of number of earthquakes, energy released (4E+19 erg) and areal extent (~60 km^2). It contains 30 events with $M_L \geq 3.0$ occurred from October 2011 to May 2014, which also includes the main earthquake of the whole Pollino seismic activity (25 October 2012, M_L5; M_w5.2). Cluster 1 shows a peculiar triangular shape elongated for about 12 km in the N-S direction. Westward is confined by the Easternmost segment of the East-dipping CRFS, Eastward by the West-dipping RSB-VCT (ROCS) and Southward by the NNE-dipping Mt. Palanuda fault (Fig. 8a). Considering the time/space evolution of the seismic activity, two sub-clusters (1-1 and 1-2 in Fig. 8) may be distinguished. Sub-cluster 1–2 contains the Mormanno main event and was activated after sub-cluster 1-1 and cluster 2. Cluster 2, also named the Morano-Calabro cluster, is located between the WSW-dipping RSB-VCT (ROCS) and the MPR fault, and extends for about 7 km in direction N-S, NNW-ward of the Morano Calabro locality. It contains fewer and less energetic events with respect to cluster 1 with the exception of the 28 May 2012, M_w 4.3 and the 6 June 2014, M_w 4.0 events, and three earthquakes with a magnitude of 3.0 ≤ M_L ≤ 3.5 which occurred from May to November 2012. Cluster 2 was almost continuously active during all the seismic crisis, with two peaks of activity in May 2012 and June 2014 (sub-cluster 2-1 and 2-2 in Fig. 8).

Eastward of cluster 2, a remarkable increase of seismic activity, with respect to the background seismicity, was observed from the beginning of 2012 with two events with 3.0 ≤ M_L ≤ 3.5 (yellow circles in Fig. 8a).

1.8. Relocated seismicity

In order to constrain the geometry of the faults possibly activated during this period of intense seismic activity, high-resolution hypocentre distributions were used. The earthquake dataset was obtained by Totaro et al. (2015), which included the events occurred from January 2010 to May 2013 and was extended, in the present study, until June 2014 (Fig. 9). It comprises all the earthquakes with a local magnitude greater than 1.0 and with a hypocentral depth lower than 30 km. Following Totaro et al. (2015), automatic and manually revised P- and S-wave arrival time picks were selected for the updated dataset (4775 earthquakes, 407 of which occurred during the last investigated year). The recording network consisted of 46 stations with epicentral distance within 150 km from the epicentres and included both the temporary and the permanent stations managed by the University of Calabria and INGV (D'Alessandro et al., 2013; Margheriti et al., 2013) Double-difference relative locations by HypoDD (v.2; Waldhauser, 2001) were computed to predict the observed data by using the 3D P-wave velocity model by Orecchio et al. (2011). Travel time differences were estimated from each event to its 30 nearest neighbours within a 10 km distance. In addition, to ensure the robustness of the double-difference inversion, only event pairs with at least eight phases observed at common stations were used. The final relocated dataset (i.e. relative to the period January 2010–June 2014) consists of 1795 events (Fig. 9a). The final dataset reliability was further checked by using the non-linear Bayloc earthquake location algorithm (Presti et al., 2004, 2008). Bayloc furnishes a probability density cloud with shape and size related to the main factors involved in the location process, for each earthquake (e.g. network geometry, picking errors). As widely documented in previous studies, the non-linear methods usually produce more realistic error estimates with respect to the linearized ones (see e.g. Husen and Smith, 2004; Lomax et al., 2000; Presti et al., 2008). The application of the Bayloc algorithm to the relocated dataset, furnishes horizontal and vertical errors of the order of 1.25 and 1.80 km respectively, thus confirming the reliability of our results and the stability of the main features revealed by the seismicity distribution.

2. Discussion

2.1. Geometric relationships and hierarchy of the quaternary faults

In the Mercure-Pollino region, with missing subsurface data, an attempt to reconstruct the structural style and evolution of the extensional system can only be based on the geometry, the kinematics and the timing of the E-dipping (CRFS) and W-dipping (ROCS, MPR and SVPC) fault sets, (Figs. 2 and 5 and Table 1).

In particular, taking into account the previously discussed data, the following is noted:

- All the E-dipping faults of the CRFS are sub-parallel in strike and show a nearly constant, dip-slip kinematics, suggesting they originated in response to the same, long-lasting, extensional deformation field, with an average WSW-ENE trending T-axis. A co-axial deformation field is derived from the fault slip data collected on the West-dipping faults surveyed during our fieldwork (T-axes contour diagrams of Fig. 5).
- The E-dipping faults of the CRFS have lower dip-angles (from 20° to 75°, steepening from West to East) than the W-dipping VCT, RSB, MPR and VPP faults (from 55° to 80°, Fig. 3b).
- The GCG E-dipping fault shows the lowest dip-angle (20°) and the largest along-dip geological displacement associated with a single fault (~2600 m); this fault can be considered the master fault of the entire examined system.
- The cumulated geological displacement of the whole CRFS (i.e. the sum of the displacements of all the faults) is larger (~3850 m) than the cumulated displacement measured for the antithetical structures (~2400 m).
- Due to the lower dip-angle of the E-dipping faults, the dip-parallel displacement results in a larger cumulated heave (~3150 m) compared to the heave produced by the antithetical faults (~950 m). Conversely, the cumulated throw along the W-dipping faults (~2250 m) exceeds the cumulated throw associated to the CRFS (~1850 m). Therefore, the E-dipping fault set contributed much more than the antithetical set in terms of the overall deformation which occurred from the beginning of the extensional phase (Early Pleistocene).
- The stratigraphic morpho-structural data suggests that the CRFS faults originated following an Eastward-younging trend, from the Early-Middle Pleistocene (GCG and PPS faults) to Middle-Late Pleistocene (AVN and BAT faults) and that the two Easternmost structures could be presently active (Table 1).
- The ROCS, the MPR and the SVPC show local field evidence of very recent movements (Late Pleistocene – Holocene age).

2.2. Asymmetric extension model

The above geometric-kinematic setting fits a regional model of asymmetric extension, ultimately driven by the East-dipping CRFS. In such a context, the GCG low-angle fault, that is the oldest East-dipping structure, overcoming all the others in terms of associate extension, may be interpreted as the break-away zone of an East-dipping detachment.

However, from both a geometrical and a kinematic point of view, the fault distribution observed in the study area is

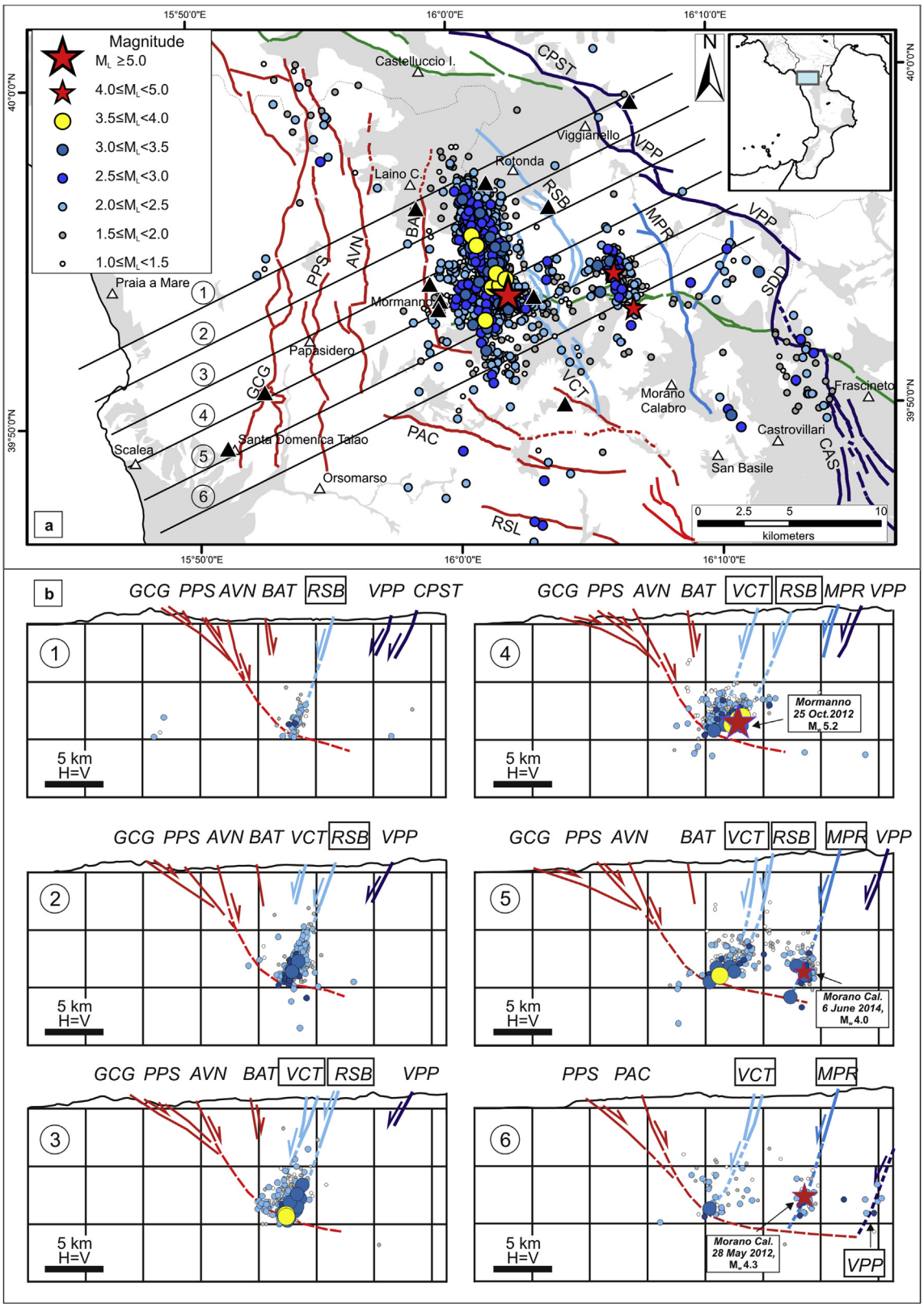

Fig. 9. Relocated seismicity occurred from January 2010 to June 2014 with local magnitude $1.0 \leq M_L \leq 5.0$ (Totaro et al., 2015 and this study) and the Quaternary and active faults in the Pollino area as derived from this study. (a) Epicentral distribution of the 1795 relocated events. Symbol shape and dimension refer to their local magnitude. The black triangles represents only the temporary and permanent seismic stations within the studied area used for locating the events and the black lines (1–6) show the trace of the cross-sections in Fig. 9b. (b) NE-SW-striking vertical cross sections displaying all earthquakes shown in map. The half-width of the projected seismicity along each section is 1 km. The positions along the profiles of the fault traces are shown with arrows plotted with their measured dip-angles. (For interpretation of the references to colour in this figure legend, the reader is referred to the web version of this article.)

inconsistent with the theoretical models of hanging wall deformation above detachment faults with a constant dip-angle (e.g. Davis, 1980; Wernicke and Burchfiel, 1982; Wernicke, 1985; Lister et al., 1986; Lister and Davis, 1989). It is known, that these low-angle extensional systems may be revealed by:

(i) domino sets bounded by synthetic faults with a uniform dip-angle,
(ii) listric fans with increasing block rotation and a decreasing fault dip-angle, moving away from the break-away, and
(iii) large roll-over anticlines with high-angle antithetic faults, to compensate volumetric problems.

Conversely, a set of synthetic splay faults, which steepen moving-away from the break-away zone, as observed in the CRFS, is what was expected above a detachment, characterized by a progressive downward increase of the dip-angle, at least from the shallower crustal levels, down to 8–10 km.

The resulting upward-convex geometry is hardly interpretable as a primary feature. It could be due to a readjustment of the break-away zone (GCG) in response to the high displacement value and the consequent hanging wall unloading. The latter could have caused the isostatic uplift of the footwall block and induced the progressive warping of the main fault plane, leading to the subsequent deactivation of its shallower and Westernmost sector.

In our opinion, this model seems to fit the time-space evolution observed within the CRFS. In fact, the progression of the hanging wall collapse, from West to East, could have caused the abandonment of the Westernmost and oldest structures, e.g. the GCG and the PPS (Early-Middle Pleistocene), transferring the deformation to the Easternmost synthetic splay faults (AVN and BAT), active from Middle Pleistocene to present.

The proposed interpretation has the advantage to frame all the mapped extensional fault sets including their evolution in a coherent regional tectonic-kinematic model. However, due to the lack of subsurface data, alternative models may be applied also by exploiting the same seismological dataset. It is not surprising, that Totaro et al. (2015) correlated the Pollino seismic sequence to West dipping faults, which were supposed to be blind and to root into a West-dipping detachment. It should be noted that these authors did not have detailed structural data in the Pollino epicentral area and that they referred to regional studies, concerning the active fault patterns (Fig. 1c), to draw an interpretative regional section (Menardi Noguera and Rea, 2000; Mazzoli et al., 2008) which is located tens of kilometres Northward.

Ought to be taken into account that the assumption of a West-dipping basal detachment, for the faults activated by the Pollino seismic activity, opens the problem of the role of the CRFS faults. The latter would be in fact downgraded to antithetical structures, in spite of their predominant values of displacement (Table 1).

2.3. Earthquake/fault association

The 2010–2014 Pollino seismic activity originated in response to a SW-NE tensional state of stress in the Southern part of the Apennines active extensional belt (Fig. 1). This is highlighted by the focal mechanisms of the three major events (the Mormanno Earthquake, 25 October 2012, M_w 5.2, the Morano Calabro Earthquake 28 May 2012, M_w 4.3 and the Morano Calabro Earthquake 6 June 2014 Mw 4.0) and of other seven $M_w \geq 3.5$ events (Fig. 8a). All these earthquakes are of extensional type with WSW- ENE oriented T-axes. Such a tensional axis is also near co-axial with the geological and seismological stress tensors derived by Brozzetti et al. (2009) in the Mercure area, as well as with the orientation of the active minimum compression axis from borehole breakouts (Montone et al., 2004; Pondrelli et al., 2006), and with GPS recent data (D'Agostino et al., 2013).

It is also co-axial with the average T-axis derived from the fault slip data collected on both the East- and West-dipping faults (Fig. 5).

The attitude of the West-dipping seismogenic planes, highlighted from the Pollino 2010–2014 focal solutions is very similar to that of the fault segments in the epicentral area and nearly parallel to the direction of the maximum elongation of the two major Mormanno and Morano Calabro clusters of the seismic events (Fig. 8). The general consistence between field and earthquake data support seismogenic sources ranging in strike from N-S to NNW-SSE, and dipping to the West. This inference is coherent with the analysis of an updated dataset of 1795 events with $M_L \geq 1.0$ (mean horizontal and vertical formal errors of approximately 1.25 and 1.80 km, respectively) relocated by Totaro et al. (2015) and partly in this study (Fig. 9). In this paper, the geometry of the seismogenic sources associated to the Pollino seismic activity was reconstructed analyzing the seismicity distribution, at depth, along six narrowly spaced vertical SW-NE cross-sections, and its correlation with the newly found active faults (Fig. 9). These latter, in the sections, are reported at surface with the outcrop dip-angles and are interpreted in the subsurface according to an asymmetrical extension model that is coherent with the geological constraints previously discussed. Among the active faults highlighted in this paper (Figs. 2 and 9), a good candidate as a likely seismogenic source for the 25 October Mormanno Earthquake (M_w 5.2) is the WSW-dipping Rotonda-Campotenese fault set (ROCS), which consists of the RSB and VCT en echelon coalescent segments and, at the surface bounds Eastward Cluster 1 (Figs. 8 and 9a).

In the two Northernmost transects (1 and 2 in Fig. 9b), it is evident that the seismicity, at depths between 5 and 10 km, is well correlated with the Northernmost strand of the RSB fault segment. The RSB shows at the surface an average dip of 70°–75° and at depth a dip of approximately 55° delineated by low magnitude events, mostly less than M_L 3.0.

The two central transects (3 and 4 in Fig. 9b) show that both the VCT and RSB segments are involved in the Cluster 1 seismic activity. The two segments are clearly distinct at surface, whereas at a depth of approximately 9 km, they tend to merge. The envelop of the seismic events correlated with the RSB segment contains the most energetic event (Mormanno, 25 October 2012, M_L5; M_W 5.2) as well as other significant earthquakes, whereas only minor seismicity appears to be associated with the VCT segment. It worth noting that the base of the Cluster 1 rock volume is close to the possible intersection with the down-dip prolongation of the East-dipping AVN fault (Fig. 9). A temporary activation of a small AVN strand, close to the intersection with VCT, during the initial stages of the seismic activity, could also be taken into consideration. This is based on the NNE-SSW average epicentral strike of Cluster 0, co-axial to the AVN strike (Fig. 8a), and on the slight Eastward dip of the associated hypocenter, located at depths of approximately 7–9 km Westward of the Mormanno Earthquake (See section 3). It is however necessary to take into account that the low magnitudes of the events characterizing Cluster 0 and the angular coverage of the seismic network in 2010, during this early stage of the seismic activity, does not allow to fully prove this hypothesis.

The identification of the fault segment causative of the Morano-Calabro cluster (Cluster 2) and of its two major events (28 May 2012, M_w 4.3; 6 June 2014, M_w 4.0) (Figs. 8 and 9) was more difficult, due to the more discontinuous exposition of suitable fault segments in the epicenter area (Figs. 8a and 9). Notwithstanding the distribution of the seismicity along the two Southernmost cross-sections (5 and 6 in Fig. 9b) allowed us to recognise a compatible geological structure in the WSW-dipping Morano-

Piano di Ruggio (MPR) fault. At the surface, this fault segment delimits the Eastward Cluster 2 which extends for approximately 7 km in a N170 direction (Fig. 8a). Furthermore, MPR is co-axial with the West-dipping nodal planes of the two main events of the sequence.

The inferred relationships among the major events of the Pollino seismicity and the pattern of active fault segments are schematized and summarized in the block diagram of Fig. 10. The 3D sketch was drawn in the light of the adopted structural style, characterized by an East-dipping basal detachment fault controlling the down-dip propagation of the West-dipping faults (sections of Fig. 9). To complete the seismotectonic picture, the macroseismic epicenters of the major historical events located within the study area ($M_w \geq 4.5$) are also displayed in Fig. 8. Of course, it should be kept in mind the fact that we are considering historical earthquakes which occurred between the end of 17th and the beginning of the 18th century, in a sparsely populated area, therefore, our consideration is only an hypothesis.

The epicenter of the 1708 earthquake, M_w 5.5 (Rovida et al., 2011) is located within the hanging wall block of the RSB, close to its Northern termination (Fig. 8), suggesting the possibility of a common seismogenic source with the Mormanno 2012 event.

The earthquake of 8 January 1693 recently relocated and dropped to a magnitude of 5.2 by Tertulliani and Cucci (2014), is located some kilometres Eastward of the Morano Calabro events, in the footwall block of the inferred seismogenic source of Cluster 2 (MPR fault, Fig. 8a), thus possibly excluding a common seismogenic source. Conversely, we further hypothesize that the 1693 event might be associated with the Southernmost segment of SW-dipping SVPC fault set, responsible for the significant paleoseismological earthquakes (500 A.D. and 900 A.D. according to Michetti et al., 1997; Cinti et al., 1997, 2002).

As previously mentioned, the Northern segment of the SVPC (CPST fault) was interpreted as the seismogenic source of the 1998 Mercure Earthquake (M_w 5.6) (Brozzetti et al., 2009).

2.4. The seismogenic style

The time-space analysis of the Pollino 2010–2014 seismic activity (Figs. 8 and 9), performed by high quality relocated earthquakes, shows that well-distinct, neighbouring and along-strike parallel earthquake clusters, related to independent fault sources, were alternatively activated by major events. In other words, the Pollino 2010–2014 seismicity activated, in a different degree and in different times, at least two sub-parallel WSW-dipping fault segments, with an along strike length of approximately 10–15 km (Fig. 9).

The observed perpendicular-to-fault strike evolution of the seismic activity is different from the along-strike one that characterized the major instrumental earthquakes which occurred in the Apennine Extensional Belt of Italy in recent years, such as the Colfiorito 1997 (M_w 6.0) and L'Aquila 2009 (M_w 6.3) events. Both these two sequences, consisting of several thousands of events, occurred on a closely-spaced adjacent en echelon fault segments, in a nearly aligned along-strike (Boncio et al., 2010; Lavecchia et al., 2012; Ferrarini et al., 2015).

It is suggested that the different evolutionary behaviour of the 2010–2014 Pollino seismicity could have been controlled by the peculiar geometric fault pattern which characterizes the area. In fact, the along-strike extent of the WSW-dipping seismogenic fault segments activated during the sequence, and especially the ROCS, responsible for the Mormanno main event, appears to be limited by the East-dipping master-fault set, which ranges in strike from North-South (AVN segment) to East-West (PAC segment) (Figs. 2 and 8).

The confinement of the W-dipping faults within the CRFS hanging wall could have hampered any further along-strike deformation. Therefore, the latter may have been forced to migrate transversely, perpendicular to the fault dip, progressively activating sub-parallel fault segments.

As an observation in support of this hypothesis, it should be

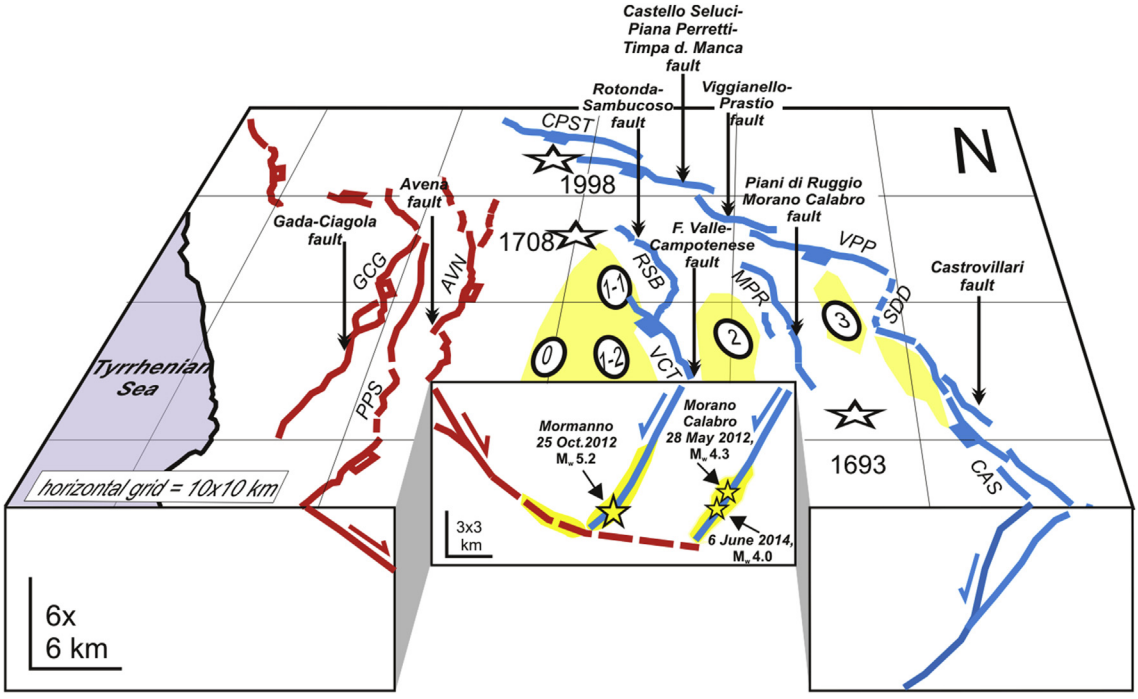

Fig. 10. 3D sketch of the active fault pattern reconstructed in the study area, with inferences on the possible association with Pollino 2010–2014 seismic activity. Faults, epicentral clusters (yellow areas) and historical earthquakes are derived from Fig.. 8 and 9; the faults are extrapolated at depth according to the structural style depicted in the sections of Fig. 9. The location of the two mainshocks of the sequence (yellow stars) is from Totaro et al. (2015); acronyms of the fault names as in Fig. 2 and Table 1. (For interpretation of the references to colour in this figure legend, the reader is referred to the web version of this article.)

noted that the ~ E-W-striking PAC is sub-parallel to the POL and, as well as this latter, it develops in correspondence of a regional-scale lineament characterized by a protracted an poly-phasic geological history.

Across this lineament, generally referred to as the "Pollino line" (Bousquet, 1971; Ghisetti and Vezzani, 1981; Knott and Turco, 1991; Van Dijk et al., 2000) the geological features change abruptly and, on the surface, the passage between the carbonate platform units and the San Donato metamorphic core occurs (Fig. 2).

It cannot be excluded that this significant geological boundary has an influence on the Southward propagation of the faults of the CRFS and ROCS, and that it drives the Eastward transfer of the active extensional belt towards the Northern Crati Graben.

3. Conclusions

The 2010–2014 Pollino seismic activity, (with the Mormanno, 2012 major event M_w 5.2) occurred close to the Lucania-Calabria border within an highly seismogenic area of the Southern Apennines of Italy (Rovida et al., 2011), also site of a possible seismic gap (Cinti et al., 2002). Therefore, such a seismic activity was particularly alarming from a seismic hazard and seismic risk point of view and the need to identify the fault system involved in the sequence was clear in order to evaluate its seismogenic potential. Previous maps of active faults (Michetti et al., 1997, 2000; Cinti et al., 1997, 2002) are not compatible with the hypo-central distribution (Fig. 1c and attached references) and it is evident that there is a lack of structural data in the epicentral area.

This paper, presents an updated structural-geological map of the Quaternary faults outcropping within an area of approximately 1200 km^2 surrounding the epicentral area, completed with fault slip data (attitude and rake), surface segmentation pattern (individual segments length), associate displacement (Geological and Late Quaternary) values and, whenever possible, slip rates (Figs. 2 and 5, Table 1).

Field and structural analysis, integrated with morpho-structural and remote sensing analysis, allowed us to detect a substantially unknown active fault system, consisting of conjugate E- and W-dipping fault sets. The East-dipping faults (eg. Coastal Range Fault Set, CRFS), which include low-angle structures (20°–40°), are interpreted as synthetic to a basal detachment outcropping in correspondence of the Gada-Ciagola LANF (GCG, Fig. 3 and 9.) and are dominant in terms of finite deformation (cumulative heave > 3000 m compared to the ~1000 m of the West-dipping faults, Table 1). The antithetic W-dipping faults, although less important in terms of long-term deformation, are however significant in controlling the Pollino 2010–2014 seismic activity. In addition, they cross-cut and displace some Early to Middle Pleistocene structures which have long been considered active and possibly seismogenic in previous studies (e.g. the CVN, which is the Westernmost continuation of the E-W Pollino fault, POL in Fig. 2), testifying that the latter cannot be considered as active in their entirety.

The epicentral area of the Pollino seismic activity is contained within a triangular zone delimited on the West and on the South by some significant faults of the East-dipping set (NNE-trending Avena fault and NNE-dipping Palanuda Mount fault) and on the East side by two of the newly identified active WSW-dipping fault set (Fig. 8), e.g. the Rotonda-Campotenese (ROCS) and the Morano Calabro-Piano di Ruggio (MPR).

Based on a good quality hypocentre location, these two faults appear suitable seismogenic sources for the Mormanno 2012 (M_w 5.2) Earthquake, nucleated at a depth of ~8.5 km, and for the Morano Calabro 2012 (M_w 4.3) and 2014 (M_w 4.0) earthquakes, nucleated at a depth of ~7.6 km and ~8.6 km respectively.

From the above considerations, it is possible to deduce that the reconstructed fault pattern, characterized by an along-strike and along-dip confinement of the most relevant West-dipping seismogenic faults (ROCS) by two nearly orthogonal fault segments of the East-dipping set (AVN and PAC, Fig. 2), suggests the existence of a physical barrier for a further along-strike growth of the ROCS with the subsequent implications on the seismic hazard of the study area.

Acknowledgments

Funding was from the DPC-INGV PROJECTS-S1 2012-2013, UR-Unich, resp. F. Brozzetti and from DiSPUTer research funds to G. Lavecchia and F. Brozzetti. We are greateful to C. Collettini, for the precious suggestion during the setting of the paper, and to F. Guzzetti for the accurate and critical review of the manuscript.

Appendix A. Supplementary data

Supplementary data related to this article can be found at http://dx.doi.org/10.1016/j.jsg.2016.10.005.

References

Amodio Morelli, L., Bonardi, G., Colonna, V., Dietrich, D., Giunta, G., Ippolito, F., Liguori, V., Lorenzoni, S., Paglionico, A., Perrone, V., Piccarreta, G., Russo, M., Scandone, P., Zanettin-Lorenzoni, E., Zuppetta, A., 1976. L'Arco calabro-peloritano nell'orogene appenninico-maghrebide. Mem. Soc. Geol. It. 17, 1–60.

Bally, A.W., Snelson, S., 1980. Realms of subsidence, facts and principles of world petroleum occurrence. In: Miall, A.D. (Ed.), Mem. Can. Soc. Pet. Geol, vol. 6, pp. 9–94.

Bingham, C., 1974. An antipodally symmetric distribution on the sphere. Ann. Statistics 2, 1201–1225.

Boncio, P., Pizzi, A., Brozzetti, F., Pomposo, G., Lavecchia, G., Di Naccio, D., Ferrarini, F., 2010. Coseismic ground deformation of the 6 april 2009 L'Aquila earthquake (central Italy, Mw6.3). Geoph. Res. Lett. 37 http://dx.doi.org/10.1029/2010GL042807.

Bousquet, J.C., 1971. La tectonique tangentielle des series calcareo-dolomitiques du nord est de l'apennin Calabro-Lucanien (Italie Méridionale). Geol. Rom. X, 23–52.

Bousquet, J.C., Gueremy, P., 1969. Quelques Phénomènes de Néotectonique dans l'Apennin Calabro-Lucanien et Leurs Conséquences Morphologiques. Rev. Géogr. Phys. Géol. Dynam 10, 225–238.

Brozzetti, F., 2011. The Campania-Lucania extensional fault system (southern Italy): a suggestion for a uniform model of active extension in the Italian apennines. Tectonics 30, TC5009. http://dx.doi.org/10.1029/2010TC002794.

Brozzetti, F., Lavecchia, G., Mancini, G., Milana, G., Cardinali, M., 2009. Analysis of the 9 september 1998 Mw 56 Mercure earthquake sequence (southern Apennines, Italy): a multidisciplinary approach. Tectonophysics 476, 210–225.

Castello, B., Selvaggi, G., Chiarabba, C., Amato, A., 2006. CSI Catalogo Della Sismicità Italiana 1981–2002. versione 1.1. INGV-CNT. http://www.ingv.it/CSI/.

Cavinato, G.P., Petronio, C., Sardella, R., 2001. The mercure river basin (southern Italy): quaternary stratigraphy and large mammal biochronology. In: The World of Elephants, Proceedings of the 1st Internationale Congress, pp. 187–190.

Chiarabba, C., Agostinetti, N.P., Bianchi, I., 2016. Lithospheric fault and kinematic decoupling of the Apennines system across the Pollino range. Geophys. Res. Lett. 43 http://dx.doi.org/10.1002/2015GL067610.

Cinti, F.R., Cucci, L., Pantosti, D., D'Addezio, G., Meghraoui, M., 1997. A major seismogenic fault in a "silent area" the Castrovillari Fault (Southern Apennines, Italy). Geoph. J. Int. 130, 595–605.

Cinti, F.R., Moro, M., Pantosti, D., Cucci, L., D'Addezio, G., 2002. New constraints on the seismic history of the Castrovillari fault in the Pollino gap (Calabria, southern Italy). J. Seismol. 6, 199–217.

Collettini, C., Sibson, R.H., 2001. Normal faults, normal friction? Geology 29 (10), 927–930.

D'Agostino, N., Avallone, A., D'Anastasio, E., Cecere, G., 2013. GPS Velocity and Strain Field in the Calabro-lucania Region. INGV-DPC Proj.1. https://sites.google.com/site/ingvdpcprojects1/documents.

D'Alessandro, A., Gervasi, A., Guerra, I., 2013. Evolution and strengthening of the calabrian regional seismic network. Adv. Geosciences 36, 11–16.

D'Amico, S., Scarfì, L., 2012. Rilievo macrosismico degli effetti prodotti dal terremoto del Pollino del 26 ottobre 2012 alle ore 01:05 locali. Report of the Quick Earthquake Survey Team, available at: www.ingv.it.

D'Argenio, B., 1992. L'Appennino Campano Lucano. Vecchi e nuovi modelli geologici tra gli anni sessanta e gli inizi degli anni ottanta. Mem. Soc. Geol. It. 41, 3–15.

Davis, G.A., 1980. Problems of intraplate extensional tectonics, western United States. In: Continental Tectonics. National Academy of Science, Washington,

pp. 84–95.
De Martini, P.M., 1996. Come colmare un gap, l'esempio di un approccio geologico nel bacino del Mercure. Relazione finale (12 pp., 8 figs) relativa alla borsa di studio in ambito Contratto CEE n. EV5V - CT 94 - 0494; Time dependent seismic hazard estimate based on multiparameter geophysical observatory system, denominato "SCENARIO".
Dietrich, D., Lorenzoni, S., Scandone, P., Zanettin, Lorenzoni, E., Di Pierro, M., 1976. Contribution to the knowledge of the tectonic units of Calabria; relationships between composition of K-white micas and metamorphic evolution. Boll. Soc. Geol. It 95, 193–217.
Ercoli, M., Pauselli, C., Forte, E., Frigeri, A., Federico, C., 2013. The Mt. Pollino Fault (southern Apennines, Italy): GPR signature of Holocenic earthquakes in a "silent" area. In: Advanced Ground Penetrating Radar (IWAGPR), 2013 7th International Workshop. IEEE, pp. 1–6. http://dx.doi.org/10.1109/IWAGPR.2013.6601510.
Faure Walker, J.P., Roberts, G.P., Cowie, P.A., Papanikolaou, I., Michetti, A.M., Sammonds, P., Wilkinson, M., McCaffrey, K.J.W., Phillips, R.J., 2012. Relationship between topography, rates of extension and mantle dynamics in the actively-extending Italian Apennines. Earth Plan. Sci. Lett. 325–326, 76–84. http://dx.doi.org/10.1016/j.epsl.2012.01.028.
Ferrarini, F., Lavecchia, G., de Nardis, R., Brozzetti, F., 2015. Fault geometry and active stress from earthquakes and field geology data analysis: the Colfiorito 1997 and L'Aquila 2009 cases (central Italy). Pure Appl. Geoph 172 (5), 1079–1103.
Ghisetti, F., Vezzani, L., 1981. Contribution of structural analysis to understanding the geodynamic evolution of the Calabrian arc (Southern Italy). J. Struct. Geol. 3 (No. 4), 371–381.
Ghisetti, F., Vezzani, L., 1982. Strutture tensionali e compressive indotte da meccanismi profondi lungo la linea del Pollino (Appennino meridionale). Boll. Soc. Geol. It. 101, 385–440.
Ghisetti, F., Vezzani, L., 1983. Structural Map of Mt. Pollino (Southern Italy). 1:50.000 Scale. SELCA, Firenze.
Giaccio, B., Galli, P., Peronace, E., Arienzo, I., Nomade, S., Cavinato, G.P., Mancini, M., Messina, P., Sottili, G., 2014. A 560-440 ka tephra record from the Mercure Basin, southern Italy: volcanological and tephrostratigraphic implication. J. Quat. Sci. 29 (3), 232–248. http://dx.doi.org/10.1002/jqs.2696. ISSN 0267-8179.
Gibbs, A.D., 1984. Structural evolution of extensional basin margins. J. Geol. Soc. Lond 141, 609–620.
Gioia, D., Martino, C., Schiattarella, M., 2011. Long-to short-term denudation rates in the southern Apennines: geomorphological markers and chronological constraints. Geol. Carp. 62, 1–15.
Grandjacquet, C., 1962. Données nouvelles sur la tectonique tertiaire des massif Calabro-Lucaniens. Bull. Soc. Geol. Fr. 7ème série 4, 695–706.
Guidoboni, E., Ferrari, G., Mariotti, D., Comastri, A., Tarabusi, G., Valensise, G., 2007. CFTI4Med, Catalogue of Strong Earthquakes in Italy (461 B.C.-1997) and Mediterranean Area (760 B.C.-1500). INGV-SGA. Available from: http://storing.ingv.it/cfti4med/.
Hunstad, I., Selvaggi, G., D'Agostino, N., England, P., Clarke, P., Pierozzi, M., 2003. Geodetic strain in peninsular Italy between 1875 and 2001. Geophys. Res. Lett. 30 (4), 1181–1184. http://dx.doi.org/10.1029/2002GL016447.
Husen, S., Smith, R., 2004. Probabilistic earthquake location in three dimensional velocity models for the Yellowstone National Park region, Wyoming. Bull. Seism. Soc. Am. 94 (6), 880–896.
Iannace, A., D'Errico, M., Vitale, S., 2004. Carta Geologica dell'area compresa tra Maratea, Castrovillari e Sangineto. In: Vitale, S., Iannace, A. (Eds.), 2004: Analisi Dello Strain Finito in 3D Dell'Unità Pollino-ciagola (Confine Calabro-lucano, Italia Meridionale). Studi Geologici Camerti. Nuova Serie, vol. 2, pp. 153–167. ISSN: 0392-0631.
Iannace, A., Garcia-Tortosa, F.J., Vitale, S., 2005. Triassic metasedimentary successions across the boundary between the southern Apennines and the Calabrian Arc (northern Calabria, Italy). Geol. J. 40, 155–171. http://dx.doi.org/10.1002/gj.1001.
Iannace, A., Vitale, S., D'Errico, M., Mazzoli, S., Di Staso, A., Macaione, E., Messina, A., Reddy, S.M., Somma, R., Zamparelli, V., Zattin, M., Bonardi, G., 2007. The carbonate tectonic units of northern Calabria (Italy): a record of Apulian palaeomargin evolution and Miocene convergence, continental crust subduction, and exhumation of HP LT rocks. J. Geol. Soc. 164, 1165–1186. http://dx.doi.org/10.1144/0016-76492007-017.
Ietto, A., Barilaro, A.M., 1993. L'Unità di San Donato quale margine deformato Cretacico-Paleogene del bacino di Lagonegro (Appennino Meridionale-Arco Calabro). Boll. Soc. Geol. It. 112, 477–496.
Ietto, A., Ietto, F., 2011. Note Illustrative Della Carta Geologica D'Italia Alla Scala 1: 50.000, Foglio 542, Verbicaro. Servizio Geologico d'Italia. Litografia Artistica Cartogr., Firenze. Available online at: http://www.isprambiente.gov.it/Media/carg/note_illustrative/542_Verbicaro.pdf.
ISIDeWorking Group (INGV), 2015. Italian Seismological Instrumental and Parametric Database. http://iside.rm.ingv.it/.
Jackson, J.A., White, N.J., 1989. Normal faulting in the upper continental crust: observations from regions of active extension. J. Struct. Geol. 11, 15–36.
Knott, S.D., Turco, E., 1991. Late cenozoic kinematics of the Calabrian arc, southern Italy. Tectonics 10 (6), 1164–1172.
Lavecchia, G., Ferrarini, F., Brozzetti, F., de Nardis, R., Boncio, P., Chiaraluce, L., 2012. From surface geology to aftershock analysis: constraints on the geometry of the L'Aquila 2009 seismogenic fault system. Italian J. Geosciences 131 (3), 330–347.
Lister, G., Davis, G.A., 1989. The Origin of metamorphic core complexes and detachment faults formed during Tertiary continental extension in the northern Colorado River region, USA. J. Struct. Geol. 11 (1/2), 65–94.
Lister, G., Etheridge, M.A., Symonds, P.A., 1986. Detachment faulting and the evolution of passive continental margins. Geology 14, 246–250.
Lomax, A., Virieux, J., Volant, P., Berge-Thierry, C., 2000. Probabilistic Earthquake Location in 3D and Layered Model, in Advances in Seismic Event Location, Pp. 101–134. Kluwer Academic Publishers, Netherlands.
Margheriti, L., Amato, A., Braun, T., Cecere, G., D'Ambrosio, C., De Gori, P., Selvaggi, G., 2013. Emergenza nell'area del Pollino: le attività della Rete Sismica Mobile. Rapporti Tecnici INGV.
Mazzoli, S., D'Errico, M., Aldega, L., Corrado, S., Invernizzi, C., Shiner, P., Zattin, M., 2008. Tectonic burial and "young" (<10 Ma) exhumation in the southern Apennines fold and thrust belt (Italy). Geology 36, 243–246. http://dx.doi.org/10.1130/G24344A.1.
Menardi Noguera, A., Rea, G., 2000. Deep structure of the campanian-lucanian arc (southern apennine, Italy). Tectonophysics 324, 239–265.
Michetti, A.M., Ferreli, L., Serva, L., Vittori, E., 1997. Geological evidence for strong historical earthquakes in an "aseismic" region; the Pollino case (southern Italy). Jour. Geodyn. 24, 67–86.
Michetti, A.M., Ferreli, L., Esposito, E., Porfido, S., Blumetti, A.M., Vittori, E., Serva, L., Roberts, G.P., 2000. Ground effects during the 9 September 1998, Mw =5.6, Lauria earthquake and the seismic potential of the "aseismic" Pollino region in southern Italy. Seism. Res. Lett. 71, 31–46.
Montone, P., Mariucci, M.T., Pondrelli, S., Amato, A., 2004. An improved stress map for Italy and surrounding regions (central Mediterranean). J. Geophys. Res. 109, B10410. http://dx.doi.org/10.410.11029/12003JB002703.
Ogniben, L., 1969. Schema introduttivo alla geologia del confine calabro-lucano. Mem. Soc. Geol. It 8, 453–763.
Orecchio, B., Presti, D., Totaro, C., Guerra, I., Neri, G., 2011. Imaging the velocity structure of the Calabrian Arc region (south Italy) through the integration of different seismological data. Boll. Geofis. Teor. Appl. 52, 625–638.
Papanikolaou, I.D., Roberts, G.P., 2007. Geometry, Kinematics and deformation rates along the active normal fault system in the southern Apennines: implications for fault growth. J. Struct. Geol. 29, 166–188.
Papanikolaou, I.D., Roberts, G.P., Michetti, A.M., 2005. Fault scarps and deformation rates in Lazio-Abruzzo, Central Italy: comparison between geological fault slip-rate and GPS data. Tectonophysics 408, 147–176.
Passarelli, L., Hainzl, S., Cesca, S., Maccaferri, F., Mucciarelli, M., Roessler, D., Corbi, F., Dahm, T., Rivalta, E., 2015. Aseismic transient driving the swarm-like seismic sequence in the Pollino range, Southern Italy. Geophys. J. Int. 201, 1553–1567.
Patacca, E., Scandone, P., 2007. Geological interpretation of the CROP-04 seismic line (southern Apennines, Italy). Boll. Soc. Geol. It. Ital. J. Geosci.) 297–315 special issue no. 7.
Pierattini, D., Scandone, P., Cortini, M., 1975. Età di messa in posto ed età di metamorfismo delle "Limburgiti" nord calabresi. Boll. Soc. Geol. It. 94, 367–376.
Pondrelli, S., Salimbeni, S., Ekström, G., Morelli, A., Gasperini, P., Vannucci, P., 2006. The Italian CMT dataste from 1977 to present. Phys. Earth Plan. Int. 159, 286–303.
Presti, D., Troise, C., De Natale, G., 2004. Probabilistic location of seismic sequences in heterogeneous media. Bull. Seismol. Soc. Am. 94, 2239–2253.
Presti, D., Orecchio, B., Falcone, G., Neri, G., 2008. Linear versus nonlinear earthquake location and seismogenic fault detection in the southern Tyrrhenian Sea. Italy. geophys. J. Int. 172, 607–618.
Roberts, G.P., Michetti, A.M., 2004. Spatial and temporal variations in growth rates along active normal fault Systems: an example from Lazio-Abruzzo, central Italy. J. Struct. Geol. 26, 339–376.
Robustelli, G., Russo Ermolli, E., Petrosino, P., Jicha, B., Sardella, R., Donato, P., 2014. Tectonic and climatic control on geomorphological and sedimentary evolution of the Mercure basin, southern Apennines, Italy. Geomorphology 214, 423–435.
Rossetti, F., Goffé, B., Monié, P., Faccenna, C., Vignaroli, G., 2004. Alpine orogenic P-T-t-deformation history of the Catena Costiera area and surrounding regions (Calabrian Arc, southern Italy): the nappe edifice of north Calabria revised with insights on the Tyrrhenian-Apennine system formation. Tectonics 23. http://dx.doi.org/10.1029/2003tc001560.
Rovida, A., Camassi, R., Gasperini, P., Stucchi, M. (Eds.), 2011. CPTI11, la versione 2011 del Catalogo Parametrico dei Terremoti Italiani, Milano, Bologna. http://dx.doi.org/10.6092/INGV.IT-CPTI11 available from: http://emidius.mi.ingv.it/CPTI (last accessed March 2014).
Schiattarella, M., 1998. Quaternary tectonics of the Pollino ridge, Calabria-Lucania boundary, southern Italy. Geol. Soc. Lond. 341–354. Spec. Publ. 135.
Schiattarella, M., Torrente, M., Russo, F., 1994. Analisi strutturale ed osservazioni morfotettoniche nel bacino del Mercure (Confine calabro-lucano). Il Quat. 7, 613–626.
Schiattarella, M., di Leo, P., Beneduce, P., Giano, S.I., 2003. Quaternary uplift vs tectonic loading: a case-study from the Lucanian Apennine, southern Italy. Quat. Int. 101–102, 239–251. http://dx.doi.org/10.1016/S1040-6182(02)00126-X.
Schiattarella, M., di Leo, P., Beneduce, P., Giano, S.I., Martino, C., 2006. Tectonically driven exhumation of a young orogen: an example from the southern Apennines, Italy. Spec. Pap. Geol. Soc. Am. 398, 371–385. http://dx.doi.org/10.1130/2006.2398(23).
Servizio Geologico d'Italia, 1970. 220 Verbicaro Sheet of the Carta Geologica D'Italia, 1. 100.000 Scale. Rome.
Servizio Geologico d'Italia, 1971. 221 Castrovillari Sheet of the Carta Geologica D'Italia, 1. 100.000 Scale. Rome.

Servizio Geologico d'Italia, 2011. Carta Geologica D'Italia Alla Scala 1:50.000, Foglio 542, Verbicaro. Available online at: http://www.isprambiente.gov.it/Media/carg/542_VERBICARO/Foglio.html.
Spina, V., Galli, P., Tondi, E., Mazzoli, S., 2009. Fault propagation in a seismic gap area (northern Calabria, Italy): implications for seismic hazard. Tectonophysics 476, 357–369.
Suppe, J., 1983. Geometry and kinematics of fault-bend folding. Amer. Jour. Sci. 283, 684–721.
Tertulliani, A., Cucci, L., 2014. New insights on the strongest historical earthquake in the Pollino region (southern Italy). Seismol. Res. Lett. 85, 743–751.
Totaro, C., Seeber, L., Waldhauser, F., Steckler, M., Gervasi, A., Guerra, I., Orecchio, B., Presti, D., 2015. An intense earthquake swarm in the southernmost Apennines: fault architecture from high-resolution hypocenters and focal mechanisms. Bull. Seismol. Soc. Am. 105, 1–6.
Van Dijk, J.P., Bello, M., Brancaleoni, G.P., Cantarella, G., Costa, V., Frixa, A., Golfetto, F., Merlini, S., Riva, M., Toricelli, S., Toscano, C., Zerilli, A., 2000. A new structural model for the northern sector of the Calabrian Arc. Tectonophysics 324, 267–320.
Waldhauser, F., 2001. HypoDD: a Computer Program to Compute Double Difference Earthquake Locations. U.S. Geol. Surv, Menlo Park, California, pp. 01–113. Open-File Report.
Wernicke, B., 1985. Uniform sense normal simple shear of continental lithosphere. Can. J.Earth Sci. 22, 108–125.
Wernicke, B., Burchfiel, B.B., 1982. Modes of extensional tectonics. J. Struct. Geol. 4, 104–115.